Chen, X., Zhu, S., Zhenin, M., Xu, W., Bose, S., Wong, M. P-F., Leung, G. P. H., Senderowitz, H., & Jeng-Haur, C. (2019). A defective flexible loop contributes to the processing and gating defects of the predominant cystic fibrosis-causing mutation. *FASEB Journal*, *33*(4), 5126-5142. https://doi.org/10.1096/fj.201801218RR

A defective flexible loop contributes to the processing and gating defects of the predominant cystic fibrosis-causing mutation

Xinying Chen[1,2,*], Siyu Zhu[1,2,*], Michael Zhenin[3], Weiyi Xu[1,2], Samuel J. Bose[4], Molly Pik-Fan Wong[1,2], George P. H. Leung[5], Hanoch Senderowitz[3] and Jeng-Haur Chen[1,2]

[1]School of Biomedical Sciences, University of Hong Kong, Hong Kong
[2]The University of Hong Kong Shenzhen Institute of Research and Innovation, Shenzhen, China
[3]Department of Chemistry, Bar Ilan University, Ramat-Gan, Israel
[4]School of Physiology, Pharmacology & Neuroscience, University of Bristol, Bristol, United Kingdom
[5]Department of Pharmacology and Pharmacy, University of Hong Kong, Hong Kong

Running title: A loop abnormality in ΔF508-CFTR

To whom correspondence should be addressed: Jeng-Haur Chen: School of Biomedical Sciences, University of Hong Kong, Faculty of Medicine Building, 21 Sassoon Road, Pokfulam, Hong Kong; jeng-haur-chen@hku.hk; Tel. +852 3917 9259; Fax. +852 2855 9730.

Footnote
*X.C. and S.Z. contributed equally to this work

ABBREVIATIONS

CF, cystic fibrosis; CFTR, cystic fibrosis transmembrane conductance regulator; IBI, interburst interval; ICL, intracellular loop; MBD, mean burst duration; MSD, membrane-spanning domain; NBD, nucleotide-binding domain; P_o, open probability; RI, regulatory insertion; RE, regulatory extension; REMD, replica-exchange molecular dynamics; RMSF, root mean square fluctuation.

ABSTRACT

People with the genetic disease cystic fibrosis (CF) often carry a deletion mutation ΔF508 on the gene encoding the cystic fibrosis transmembrane conductance regulator (CFTR) Cl^- channel. This mutation greatly reduces the CFTR maturation process and slows the channel opening rate. Here, we investigate whether residues near F508 contribute to these defects in ΔF508-CFTR. Most deletion mutations, but not alanine substitutions, of individual residues from position 503 to 513 impaired CFTR maturation. Interestingly, only protein processing of ΔY512-CFTR, like that of ΔF508-CFTR, was greatly improved by low-temperature culture at 27 °C or small molecule corrector C18. The two mutant Cl^- channels were equally slow to open, suggesting that they may share common structural flaws. Studies on the H3-H4 loop that links residues F508 and Y512 demonstrate that G509A/V510G mutations, moving G509 one position backward in the loop, markedly enhanced ΔF508-CFTR maturation and opening rate, while promoting protein stability and persistence of the H3 helix in ΔF508 NBD1. Moreover, V510A/S511A mutations noticeably increased ΔY512-CFTR maturation at 27 °C and its opening rate. Thus, loop abnormalities may contribute to ΔF508- and ΔY512-CFTR defects. Importantly, correcting defects from G509 displacement in ΔF508-CFTR may offer a new avenue for drug discovery and CF treatments.

Keywords: cystic fibrosis transmembrane conductance regulator (CFTR), ΔF508 mutation, chloride channel, low temperature and corrector C18.

INTRODUCTION

The cystic fibrosis transmembrane conductance regulator (CFTR) is a Cl^- channel on the apical membrane of epithelial cells (1, 2). CFTR is comprised of two membrane-spanning domains (MSDs) that form a transmembrane ion pathway, two nucleotide-binding domains (NBDs) that chelate and hydrolyze ATP to drive channel opening and closing, termed channel gating, and a regulatory domain that serves as a platform for PKA-dependent phosphorylation to activate the channel (3). Mutations in CFTR disrupt channel function, causing the multi-organ disease cystic fibrosis (CF) (1, 2). Currently, about 90% of people with CF carry the ΔF508 mutation, which deletes a phenylalanine residue at position 508 in NBD1 of CFTR (Fig. 1*A* and S1*A*). This mutation markedly diminishes CFTR function in epithelial cells by two major mechanisms. First, the ΔF508 mutation greatly reduces CFTR expression in the cell membrane due to impaired protein delivery from the endoplasmic reticulum (ER) to Golgi apparatus, known as the processing defect (4), and also due to accelerated ubiquitin-dependent lysosomal degradation that quickly removes any mutant proteins that reach the cell membrane (5). Second, the ΔF508 mutation slows the channel opening rate of CFTR to decrease channel activity to about only 1/4 of that in wild-type CFTR, known as the gating defect (6-9). The mutation also delays and desensitizes CFTR activation by PKA-dependent phosphorylation (10-12). These findings reveal multiple functional deficits in ΔF508-CFTR. Yet how a single residue deletion elicits such an array of abnormalities in CFTR function is not fully understood.

The ΔF508 mutation may cause dysfunction of CFTR due to loss of the backbone function (13, 14) and side-chain interactions of the F508 residue (13-16). Consistent with this scenario, protein misfolding (14, 15, 17, 18) and aberrant domain-domain interactions between NBD1 and other regions, such as intracellular loop 4 (ICL4) (14, 16, 19), ICL3 (19) and NBD2 (15), have been documented in ΔF508-CFTR. Recently solved cryo-EM structures of wild-type CFTR also reveal intensive interactions of ICL4 with F508 and nearby residues in NBD1 (20-22). In addition, impaired domain-domain interactions might accelerate ΔF508-CFTR degradation by the peripheral protein quality control mechanism (5), decrease channel thermostability (23, 24) and reduce open probability (P_o) (14, 16). Correcting individual structural defects (23, 25) seems to be a promising strategy to restore ΔF508-CFTR function. However, it is unclear whether loss of function of the F508 residue could account for all abnormalities in ΔF508-CFTR.

NBD1 crystal structures of human wild-type and ΔF508-CFTR are similar, except for the loop that connects H3 and H4 helices (H3-H4 loop) (Fig. 1*A*) (18, 26). Flexibility of the H3-H4 loop in the NBD1 crystal structure (26) or synthetic peptides (27) may be enhanced in ΔF508-CFTR. Moreover, the orientation of loop residues 509-511 is also changed in ΔF508 NBD1 (18, 26). Alterations around this loop, such as the ΔI507

mutation (28-30) or mutations of the Y512 residue (31), all impair CFTR processing. Moreover, structural differences between crystal structures of wild-type and ΔF508 NBD1 (18) might be underestimated because solubilizing mutations in these constructs partially correct ΔF508-CFTR processing and gating defects (32). The structure of ΔF508 NBD1 in the previous study (18) is found different from the recent one (33) that contains no solubilizing mutations and removes protein segments of the regulatory insertion (RI) and extension (RE). Therefore, we hypothesized that the ΔF508 mutation might cause structural abnormalities of the H3-H4 loop, as well as neighboring residues. Such alterations might contribute to functional defects of ΔF508-CFTR.

We tested this hypothesis by deleting residues near F508 and then examining their effects on CFTR processing. After discovering that the ΔY512 mutation behaved like ΔF508, we further tested whether abnormalities of the H3-H4 loop might be a mechanism that initiates both CFTR processing and gating defects.

MATERIALS AND METHODS

CFTR plasmid construction

Wild-type human CFTR in the pcDNA3.1 expression vector was a generous gift from MJ Welsh, University of Iowa. Various CFTR mutations were created using Stratagene QuickChange II site-directed mutagenesis kit (Agilent Technologies, CA) and verified by DNA sequencing.

CFTR expression and small molecule treatments

Wild-type or mutant CFTRs were transiently expressed in HeLa cells by plasmid transfection. 4 μg plasmid and 8 μl Lipofectamine 2000 (Invitrogen) were mixed in Opti-MEM I reduced serum medium (Invitrogen) and incubated with cells for 8 h at 37 ºC. Transfected cells were further cultured at 37 or 27 ºC for 40 h before harvest of proteins. CFTR correctors C4 and C18 (Cystic Fibrosis Foundation Therapeutics), each at 10 μM, were added to the culture medium 24 h before protein was harvested. All small molecules were dissolved and frozen in DMSO (x1000, 10 mM) as stocks prior to use.

Immunoblotting

The Western hybridization method was adopted from a previous study (9). After washing with ice-cold Ca^{2+}/Mg^{2+}-free PBS solution 3 times, transfected HeLa cells were digested with the lysis buffer containing 150 mM NaCl, 1% NP40 (Thermo Fisher Scientific, Waltham, MA), 1 mM EDTA, 50 mM Tris (pH 7.4), 0.1 mM phenylmethylsulfonyl fluoride (PMSF) and mixed protease inhibitors (cOmplete, Roche) for 1 h at 4 ºC. Then,

cell lysates were centrifuged at ~50,000 g (20,000 RPM) by using a Type 50.4 Ti rotor (Beckman Coulter, CA) for 20 mins at 4 ºC. The supernatant was collected and analyzed by the Bradford assay (Bio-Rad Laboratories, Hercules, CA) to determine the protein concentration. Electrophoresis of 60 or 120 µg total protein in each well was run at 150 V for 4 h in 6% SDS-PAGE gels using the Mini-Protean Tetra Cell or Protean II Xi Cell (Bio-Rad Laboratories, Hercules, CA). The running buffer contained 25 mM Tris, 192 mM glycine and 0.1% SDS.

Separated proteins in the gel were transferred to the PVDF membrane (IPVH00010, Merck Millipore, Billerica, MA) at 30 V and 4 ºC overnight, using the Tetra blotting module (Bio-Rad Laboratories, Hercules, CA) with the transfer solution containing 25 mM Tris, 192 mM glycine and 20% methanol. To detect CFTR, PVDF membranes in the 0.1% Casein blocking solution were treated with a mixture of anti-CFTR antibodies: M3A7 (Millipore), MM13-4 (Millipore, Billerica, MA) and 13-1 (R&D Systems, Minneapolis, MN) (each diluted 1:3000) for 2 h at room temperature. Then, PVDF membranes were sequentially washed 3 times with the TBST solution containing 140 mM NaCl, 0.1% Tween 20 and 20 mM Trizma (pH 7.6 with HCl), incubated with the goat anti-mouse IgG-HRP antibody (AP308P, Millipore, Billerica, MA) (1:3000 dilution) in the 0.1% Casein blocking solution for 1 h at room temperature and then washed again 3 times with the TBST solution. WesternBright ECL HRP substrate (Advansta, Menlo Park, CA) was used to illuminate CFTR. Images were captured using the ChemiDoc XRS system (Bio-Rad Laboratories, Hercules, CA) and analyzed with the software Image J (NIH). To calculate the Band C %, the background intensity was subtracted from the measured values.

Electrophysiology

CFTR currents in excised inside-out membrane patches were recorded using Axopatch 200B patch-clamp amplifiers and analyzed with pCLAMP software (both from Molecular Devices, Union City, CA), as described previously (34). The pipette (extracellular) solution contained (mM): 140 N-methyl-D-glucamine (NMDG), 140 aspartic acid, 5 $CaCl_2$, 2 $MgSO_4$ and 10 TES, pH 7.3 with Tris ([Cl^-], 10 mM). The control bath (intracellular) solution contained (mM): 140 NMDG, 3 $MgCl_2$, 1 CsEGTA, 5 Trizma base and 5 Bis-Tris, pH 7.3 with HCl, ([Cl^-], 147 mM; free [Ca^{2+}], $<10^{-8}$ M) at room temperature.

The channel activity of CFTR in excised inside-out membrane patches was activated and maintained by adding PKA (75 nM) and ATP (1 mM) to the bath solution in the recording chamber (Brook Industries, IL, USA). Membrane voltage was clamped at –50 mV. For data analysis and storage, CFTR currents were filtered with an 8-pole Bessel filter (model 900; Frequency Devices, Inc., Ottawa, IL) at a corner frequency (f_c) of 500

Hz and acquired using a Digidata 1440 interface (Molecular Devices) and pCLAMP software at the sampling rate of 10 kHz.

For analyzing the patch-clamp data, the number of active channels (N) in a membrane patch was determined by the maximum number of recorded channels that opened simultaneously at any one time during the entire experiment. For open probability (P_o) and burst analysis, event lists of open- and closed-times were created using pCLAMP software with a half-amplitude crossing criterion. Transitions ≤ 1 ms were excluded from event lists (eight-pole Bessel filter rise time ($T_{10\text{-}90}$) ~0.73 ms at f_c = 500 Hz).

To measure mean burst duration (MBD), interburst interval (IBI) and P_o within a burst ($P_{o\text{-burst}}$), burst analysis was performed using recordings from membrane patches that contained 1-4 active channels. The delimiter time (t_c) that separates interburst closures from intraburst closures was determined from the point of intersection between the two exponential curves fitting fast and slow populations of channel closures in the closed-time histogram, as described previously (35). Event lists and t_c values were used to derive MBD and $P_{o\text{-burst}}$ with pCLAMP software. To obtain burst durations, opening bursts formed by only one active channel were measured. Finally, IBI was calculated using the equation:

$$P_o = \frac{MBD \times P_{o\text{-burst}}}{MBD + IBI}$$

To obtain N accurately, the time required to observe an event where all active channels open simultaneously was estimated by the equation: $(3\times\tau_o/N)/(P_o)^N$ (36), in which the open time τ_o could be estimated by MBD. For wild-type CFTR with P_o = 0.39 and MBD = 401 ms (Fig. 4*C*, *D*), it requires ~13 s for observing all 4 channels opening at the same time and ~27 s for 5 channels. Moreover, for ΔF508/AG (G509A/V510G)-CFTR with P_o = 0.21 and MBD = 351 ms (Fig. 6*C*, *D*), it requires ~2.3 mins for N = 4 and ~8.6 mins for N = 5. Thus, we recorded CFTR currents in the presence of ATP (1 mM) and PKA (75 nM) for 6-30 mins for most experiments. To maintain channel activity, we replaced the bath solution with fresh ATP and PKA after recording for 15 mins. However, N would be underestimated for mutant CFTR with large gating anomalies such as ΔF508- and ΔY512-CFTR. Therefore, reported P_o of these two CFTR mutants could be considered as maximum P_o and their IBI as minimal IBI.

For the purpose of illustration, recordings were further digitized at 1 kHz, in which current tracings of 10 s could clearly demonstrate the gating kinetics of CFTR with reduced data points, noise and some very brief current transitions (e.g., those < 1 ms).

Molecular dynamics simulation

Simulations were performed for ΔF508-G509A/V510G human ΔRI, ΔRE-NBD1, comprising residues 387-646 (excluding a deletion of residues 405-436) with no additional solubilizing mutations (PDB entries 2PZF, 2.0 Å resolution). This structure was solved by introducing G509A and V510G mutations into the crystal structure of ΔF508 NBD1 (PDB: 2PZF) with conformational optimization of neighboring residues within a distance of 5 Å using software Discovery Studio 2018 (37). To incorporate ATP and Mg^{2+} into the structure, the parameters for ATP were obtained from the OPLS/AA force field as implemented in Schrodinger (Schrodinger Maestro, 9.0; Schrodinger: NY, 2009) while those for Mg^{2+} are included in the GROMACS implementation of this force field. Similar trajectories obtained for wild-type and ΔF508-NBD1 were adopt from the previous study (38).

Replica-exchange molecular dynamics (REMD) simulation was performed using the GROMACS package as described previously (38). In brief, the construct was simulated three times each time starting from a different random seed. The simulation consisted of 32 replicas covering a temperature range of 300 °K (26.85 °C) to 349.38 °K (76.23 °C) with each replica running for 10 ns. Thus, the construct was simulated for a total of 960 ns (32 replicas x 10 ns x 3 times).

All analyses were performed on the lowest temperature (ground state) replicas. The dynamic behavior of the protein was evaluated by calculating the root mean square fluctuation (RMSF) profile for each trajectory. Prior to RMSF calculation, the entire trajectory was superposed on the starting structure using all backbone atoms. The dynamics of a residue was defined to be significantly different between two constructs (e.g., between ΔF508 and ΔF508/AG NBD1) when RMSF values of the residue were consistently higher or lower in one construct than those in the other construct across all three simulation repeats. To predict and compare the secondary structure propensity of a polypeptide segment across the different constructs, a comparative analysis of the trajectories was performed using the dictionary of secondary structure of proteins (DSSP) algorithm.

Reagents, chemicals and resources

CFTR correctors are generously provided by the Chemical Compound Distribution Program from Professor Robert J. Bridges, Rosalind Franklin University of Medicine and Science, and Cystic Fibrosis Foundation Therapeutics. PKA purified from bovine heart was purchased from Calbiochem/Merck Millipore (Darmstadt, Germany). Stock solutions of ATP were prepared fresh before each experiment. Except for those indicated in the text, all other chemicals were purchased from Sigma (Sigma-Aldrich China, Shanghai, China) in reagent grade. PyMOL software (http://www.pymol.org), a molecular visualization system, was used for preparing all structural figures.

Statistics

Results are expressed as means ± S.E.M. of n observations. In immunoblotting experiments, n represents the number of immunoblots and in electrophysiological experiments, n represents the number of individual membrane patches obtained from different cells. One-way ANOVA was used to analyze sets of data. Differences were considered statistically significant when $P<0.05$.

RESULTS

The F508 residue is located at the end of the H3 helix in NBD1 of human CFTR and connects the H4 helix via a flexible loop structure (H3-H4 loop) (Fig. 1*A*, S1*A*) (18, 21, 26). Although deletion of this residue (ΔF508) severely impairs CFTR function (4), it shows small impacts on the crystal structure of wild-type NBD1, except residues 509-511 of the H3-H4 loop (Fig. 1*A*) (18, 26, 33). Interestingly, the NMR spectroscopy study (39) demonstrates that phosphorylation-induced conformational changes in wild-type and ΔF508 NBD1 are different and that the differences extend beyond the immediate neighborhood of F508. These findings may suggest that if residues match at the level of the crystal structure, it does not necessarily indicate that they also match when protein flexibility is introduced. Therefore, differences in conformation and function of wild-type and ΔF508 NBD1 may exist *in vivo*, contributing to ΔF508-CFTR dysfunction (e.g., the protein processing defect (4)). To test this hypothesis, we first asked whether residues near F508 play an important role in CFTR processing.

Effects of residue deletions or substitutions near F508 on CFTR processing

We began by individually deleting residues within positions 491 to 525 (Fig. 1*A*) and examining protein expression of these CFTR mutants (Fig. 1*B, C*). Our data demonstrate that ΔV510- and ΔS511-CFTR expressed relatively abundant protein in the Band C form (Band C % = $\frac{C}{B+C}$ %, Fig. 1*B, C*), which may contain fully glycosylated CFTR present in the Golgi network and cell membrane as described previously (28). By

contrast, all other mutants including ΔF508-CFTR displayed proteins mostly in the Band B form (Fig. 1*B*, *C*), representing core glycosylated CFTR in the ER membrane (28). These data indicate that except for ΔV510 and ΔS511, residue deletions near F508 greatly impaired CFTR processing.

From a structural standpoint, removing a residue from a polypeptide chain may lead to two major alterations: shortening the peptide chain and removing side-chain interactions of the residue (13). Following this conceptualization, we used alanine substitutions at each residue from position 503 to 513 (Fig. 2*A*) to retain the length of the peptide chain while disrupting side-chain function of the residue for assessing their effects on CFTR processing. The data showed that Band C expression was profoundly decreased by the N505A mutation (Fig. 2*A*), moderately reduced by D513A, and little diminished by K503A, F508A and Y512A (Fig. 2*A*). Of note, Band C % of I507A-CFTR was 92.2 ± 0.5% (N = 6), similar to that of wild-type CFTR (P>0.05, one-way ANOVA). Interestingly, substitutions of the N505 residue with 8 other different residues all largely decreased Band C % (Fig. 2*B*). Thus, these data suggest that side chains of N505 and D513 residues are required for normal CFTR processing.

To better understand underlying mechanisms, we sought clues from side-chain interactions of these two residues with other regions in CFTR (Fig. 2*C*, S1*B*, S2*C*, S3*E*). The human NBD1 structure (Fig. 2*C*, S2*C*) (18, 21) reveals that the side chain of N505 interacts with the backbone of M498 and the side chain of R560. Therefore, to test whether intradomain interactions among these three residues are important for CFTR processing, site-directed mutations were made at these sites (Fig. 2*D*). We found negligible effects of M498A and M498F mutations on Band C % (Fig. 2*D*). By contrast, the M498P mutation, which might alter backbone conformation, greatly decreased Band C % (Fig. 2*D*). Moreover, profound reductions in Band C % were also observed in R560A-, R560N- and N505R/R560N-CFTR (Fig. 2*D*). These data suggest that precise intradomain interactions among these three residues N505, M498 and R560 may be required for normal CFTR processing.

In addition, the side chain of D513, which is located on the surface of NBD1 (Fig. 1*A*, S3*E*), weakly interacts with residues S511, Y512, R516 and Y563 at long distances (Fig. S1*B*, S3*E*) (18, 21) and is far from residues in other CFTR domains (Fig. S3*E*) (21). Thus, we hypothesized that negative charge at this position may contribute to the structural integrity required for protein processing. The data demonstrate that additional mutations of D513 with the negative glutamate (D513E), positive lysine (D513K) and neutral leucine residue (D513L) showed little, moderate and large reductions in Band C %, respectively (Fig. 2*E*). Band C % of D513K- (Fig. 2*E*) and D513A-CFTR (Fig. 2*A*) were similar, whereas both were smaller than that of D513E-CFTR (Fig. 2*E*; P<0.05, one-way ANOVA), consistent with our hypothesis.

Taken together, these data suggest that normal CFTR processing requires integrity of all tested residues near F508 (Fig. 1) and proper side-chain interactions from D513 and N505 residues (Fig. 2). For those residues whose deletion, but not alanine substitution, strongly diminished CFTR processing (Figs. 1*C*, 2*A*), loss of backbone function at these positions might be a dominant factor contributing to the CFTR processing defect.

ΔY512-CFTR processing is enhanced by low temperature and CFTR correctors

Although our study identified deletion mutants near F508 affecting CFTR processing, it is unclear whether they have a similar mechanism of dysfunction as ΔF508-CFTR. We reasoned that if a deletion mutation impairs CFTR function by the mechanism similar to that of ΔF508, protein expression of this mutant may be enhanced by treatments well-known to rescue ΔF508-CFTR processing (Fig. 3), such as the low-temperature culture at 27 °C (40) and CFTR correctors C4 (compound 4a) (41) and C18 (25, 29).

Figure 3*A* demonstrates that after transient expression in HeLa cells for 40 h, ΔF508- and ΔY512-CFTR cultured at 27 ºC displayed Band C % larger than that at 37 ºC (Fig. 3*A*). Moreover, the low-temperature culture modestly enhanced Band C % of ΔV510- and ΔS511-CFTR, but slightly decreased Band C % of wild-type CFTR (Fig. 3*A*) and was without effects on other deletion mutants (Fig. 3*A*). Similarly, 24 h incubation with corrector C18 at 37 ºC greatly increased Band C % of ΔF508- and ΔY512-CFTR (Fig. 3*B*) and enhanced that of ΔV510- and ΔS511-CFTR (Fig. 3*B*), compared to that without treatment (blank columns, Fig. 3*B*). These data suggest that ΔY512 and ΔF508 mutations may impair CFTR processing by similar mechanisms, which can be rescued with low temperature or corrector C18.

We also noted that DMSO (0.1%) alone at 37 ºC significantly enhanced Band C % of ΔV510- and ΔS511-CFTR about 1.2- and 1.3-fold (blank columns, Fig. 3*A, B*, $P<0.05$, one-way ANOVA). We speculate that DMSO enhanced Band C % of ΔV510- and ΔS511-CFTR possibly by acting as a chemical chaperone (42, 43).

To investigate possible differences between processing defects of the ΔF508- and ΔY512-CFTR, we performed combination treatments on these and additional deletion mutants (Fig. 3*C, D*). The data demonstrate that compared to the vehicle control of 0.1% DMSO at 37 ºC, low temperature or the combination of low temperature and corrector C18 showed no apparent increases in Band C % of ΔI506-, ΔG509-, ΔV510-, ΔS511- and ΔD513-CFTR (grey and green columns, Fig. 3*C*). Since the individual treatment of low temperature or corrector C18 at 37 ºC enhanced Band C % of ΔV510- and ΔS511-CFTR (Fig. 3*A, B*), these data suggest that DMSO, low temperature and corrector C18 might have enhanced protein processing of these two mutants by

similar mechanisms (Fig. 3*A, C*), whereas corrector C18 exerted additional effects on these two mutants at 37 ºC (Fig. 3*B, C*).

Conversely, low temperature and corrector C18 either alone or together enhanced Band C % of ΔF508- and ΔY512-CFTR (Fig. 3*C*). By close inspection, we found that the combination treatment promoted an additive increase in Band C % of ΔF508-CFTR, compared to individual treatments (Fig. 3*C*). However, the combination treatment only caused a small synergistic enhancement in Band C % of ΔY512-CFTR (Fig. 3*C*). It is also important to highlight that Band C % of ΔY512-CFTR was higher than that of ΔF508-CFTR at 37 and 27 ºC with or without 0.1% DMSO in the culture medium (Fig. 1*C*, 3*A*, 3*C*, 3*D*, $P<0.05$, one-way ANOVA). Thus, these findings suggest that subtle differences exist between ΔF508- and ΔY512-CFTR in response to low temperature and corrector C18.

Recent studies indicate that the F508 residue mediates NBD1-MSDs interactions (Fig. S2*F*) (20, 21), which are disrupted by the ΔF508 mutation (14, 16, 19) but restored by corrector C18 in ΔF508-CFTR (25). However, the F508 residue is unchanged in ΔY512-CFTR and the Y512 residue mostly participates in intradomain interactions (Fig. S1*C*, S3*D*) (21). Therefore, it is possible that corrector C18 may rescue ΔY512-CFTR processing by another mechanism related to low temperature-mediated correction.

To further investigate differences in the processing defect between ΔF508- and ΔY512-CFTR, we tested these two mutants with CFTR correctors C4 and C18 together at 27 ºC (Fig. 3*D*). Our data demonstrate that at 27 ºC, correctors C4 and C18 caused additive increases in Band C % of both mutants (Fig. 3*D*). However, corrector C18 exhibited stronger effects than corrector C4 in ΔF508-CFTR (green and black columns, Fig. 3*D*, $P<0.05$, one-way ANOVA), whereas correctors C4 and C18 alone caused similar stimulations of Band C % for ΔY512-CFTR (Fig. 3*D*). Different responses to correctors C4 and C18 between ΔF508- and ΔY512-CFTR (Fig. 3*D*) suggest that the processing defect of these two mutants may share common mechanisms, although to varying degrees.

We next asked whether channel gating of ΔY512-CFTR may display defects similar to those of ΔF508-CFTR (6-8).

ΔY512-CFTR gating exhibits low P_o and prolonged IBI

We studied the single-channel activity of 4 deletion mutants: ΔF508-, ΔV510-, ΔS511- and ΔY512-CFTR (Fig. 4*A*) that had sufficient protein expression in the cell membrane at 37 or 27 ºC for patch-clamp experiments

(Figs. 1*B* and 3*A*). As described in the Methods, we made prolonged, uninterrupted recordings at room temperature, where ΔF508-CFTR channel activity is stable (e.g., 44), to accurately determine channel number and acquire sufficient transitions to quantify channel gating. The single-channel current amplitude (i) of these 4 deletion mutants were similar to that of wild-type CFTR (Fig. 4*B*). However, the open probability (P_o) (Fig. 4*C*) and mean burst duration (MBD) (Fig. 4*D*) of ΔV510-CFTR were moderately lower than those of wild-type CFTR. Importantly, the P_o of both ΔF508- and ΔY512-CFTR were greatly decreased (Fig. 4*C*) due to profound prolongations of the interburst interval (IBI) (Fig. 4*E*). The data showed that deletions in the H3-H4 loop that links the F508 and Y512 residues (Fig. 1*A*, S1*A*) may alter CFTR gating. These data also revealed that ΔF508 and ΔY512 mutations caused similar gating defects of CFTR.

The similarity of CFTR processing and gating defects between ΔF508- and ΔY512-CFTR (Fig. 3 and 4) suggests that the H3-H4 loop might be dysfunctional in these two mutants. In support of this idea, only those CFTR mutants with deletions in the loop, including ΔV510-, ΔS511- and ΔY512-CFTR except for ΔG509-CFTR, showed improvement in protein processing by low-temperature culture or corrector C18 (Fig. 3*A* and *B*). Previous studies (18, 26) also demonstrate that the orientation of residues 509-511 in ΔF508 NBD1 is dramatically different from that of wild-type NBD1. Thus, it is possible that abnormality of the H3-H4 loop may offer a common defect to both ΔF508- and ΔY512-CFTR, although ΔF508 and ΔY512 mutations may impair loop structure and function differently.

Deletion of a residue in the H3-H4 loop alone may not play a major role because removing either the V510 or S511 residue only moderately reduced CFTR processing (Fig. 1*C*) and was without effects on IBI (Fig. 4*E*). The data suggest that additional defects from loop residues may impair function of ΔF508- and ΔY512-CFTR. To test this hypothesis, we replaced loop residues G509, V510 and S511 in ΔF508- or ΔY512-CFTR with alanine or glycine to alter properties of these loop residues (Fig. 5*A*, *B*). Notably, here we assume that ΔF508- and ΔY512-CFTR defects are associated with conformational changes of amino acid residues in the loop, regardless of other factors such as the effect of the mRNA sequence on protein processing (45).

Displacement of G509 in ΔF508-CFTR and the missing side chain of Y512 in ΔY512-CFTR caused the severe processing defect

The amino acid sequence of the H3-H4 loop of ΔF508-CFTR could be considered the same as that of ΔV510-CFTR with two additional mutations F508G and G509V. Here we assume: ΔF508-CFTR = ΔV510-F508G/G509V-CFTR. In other words, we propose that the ΔF508-CFTR processing defect is generated from three structural alterations: ΔV510, F508G and G509V. Therefore, the huge difference in Band C % of ΔV510-

CFTR ~ 67% and ΔF508-CFTR ~ 4% (Fig. 1*C*) may be resulted from mutations F508G and G509V in ΔV510-CFTR. Furthermore, four structural changes in the residue by these two mutations were noted: (1) F508G removes the side chain of F508 and (2) inserts the special residue glycine; (3) G509V introduces the side chain of valine while (4) replacing the specific side chain (hydrogen) of glycine. Thus, we hypothesized that these four structural changes may lead to a ~ 63% reduction in Band C % of ΔF508-CFTR.

To test these four mechanisms, we used the mutation G509A that removes special properties of the glycine residue, such as the high conformational flexibility and helix breaker, at F508G (mechanism 2, lane 1, Fig. 5*A*) and V510A that eliminates interactions from valine's side chain (mechanism 3, lane 2, Fig. 5*A*). The data indicate that G509A, V510A or the double mutation (lane 3, Fig. 5*A*) showed no apparent improvements in Band C % of ΔF508-CFTR, arguing against mechanism 2 and 3. To test mechanism 1, the F508 residue was introduced back to the normal position in ΔV510-F508G/G509V-CFTR to form ΔV510-G509V-CFTR, whose amino acid sequence is identical to that of ΔG509-CFTR. As ΔG509-CFTR exhibited a severe processing defect (Fig. 1*B, C*), mechanism 1 may not be supported by our data.

Therefore, we further examined mechanism 4 by introducing glycine back to the normal position (lane #4, Fig. 5*A*, the ΔF508-G509A/V510G mutation) and found that it markedly enhanced CFTR Band C % to about 57%, close to 67% in ΔV510-CFTR (Fig. 1*C*). These data suggest that moving the G509 residue back to its normal position in ΔF508-CFTR corrects a major part of the processing defect. We speculate that the rescue effect of G509A/V510G mutations is associated with benefits from alterations of loop properties or with alleviation of structural flaws brought about by the ΔF508 mutation.

Considering the marked difference in Band C % between ΔF508-G509A/V510A-CFTR (lane #3, Fig. 5A) and ΔF508-G509A/V510G (ΔF508/AG)-CFTR (lane #4, Fig. 5A), moving the glycine residue backward to the V510 position (V510G) in ΔF508-CFTR may play a critical role in improving protein expression. Two possible effects may exist: (1) the glycine residue increases flexibility of the local loop structure or (2) it restores formation of the normal H3 helix due to its specific function as the helix breaker. To test the first hypothesis, the loop flexibility was further increased by re-introducing G509 back to position 508 (lane #5, Fig. 5*A*, the ΔF508-V510G mutation), which actually decreased Band C %, compared to that of ΔF508/AG-CFTR (lane #4, Fig. 5*A*, $P<0.05$, one-way ANOVA). These data suggest that glycine at position 508 in ΔF508-CFTR may disrupt protein processing. Moreover, adding another glycine at position 510 (S511G, lane #6, Fig. 5*A*) further decreased Band C %, compared to that at lanes #4 or #5 ($P<0.05$, one-way ANOVA). By contrast,

adding V510G or V510G/S511G mutations to wild-type CFTR was without effects on Band C % (lanes #7-8, Fig. 5*A*).

These data suggest that increasing loop flexibility by glycine substitutions is not beneficial for ΔF508-CFTR processing, but also not harmful for wild-type CFTR expression. Therefore, restoring G509 position in the H3-H4 loop, but not increasing flexibility, may account for the enhanced Band C % of ΔF508/AG-CFTR. Furthermore, we speculate that the proper length or persistence of the H3 helix would be required for correcting the processing defect of ΔF508-CFTR.

On the other hand, the amino acid sequence of the H3-H4 loop of ΔY512-CFTR is the same as that of ΔV510-S511V/Y512S-CFTR. Therefore, the difference in Band C % of ΔY512- and ΔV510-CFTR (Fig. 1*C*) could result from alterations in side-chain interactions of S511 and Y512 residues. With alanine substitutions to remove side-chain interactions of the replaced residue, our analysis showed that V510A, S511A, V510A/S511A and additional G509A/V510A mutations in ΔY512-CFTR did not promote Band C % (lanes #1-4, Fig. 5*B*).

Conversely, restoration of Y512 back to its normal position creates ΔV510-S511V-CFTR, the same as ΔS511-CFTR, which showed protein processing similar to that of ΔV510-CFTR (Fig. 1*B, C*). Because the Band C % of Y512A-CFTR was relatively good (Fig. 2*A*), these data suggest that the side chain of Y512 is important for CFTR processing only when the loop is shortened by deletion of a residue. As the phenyl ring of Y512 weakly interacts with the side chain of I507 in the H3 helix and E514 and Y515 in the H4 helix (Fig. S1*C*, S3*D*) (21), we speculate that these side-chain interactions may be important for maintaining the structural integrity of NBD1 while the loop is shortened.

Since low temperature and corrector C18 enhanced CFTR processing only for some deletion mutants in the H3-H4 loop (Fig. 3*A, B*), we next asked whether loop mutations alter their effects on ΔF508- and ΔY512-CFTR processing.

Loop mutations alter the rescue effect of low temperature and corrector C18 on ΔF508- and ΔY512-CFTR processing

To test this hypothesis, we examined the effects of low temperature, corrector C18 or the combination treatment on Band C % of ΔF508/AG-CFTR and ΔY512-V510A/S511A (ΔY512/2A)-CFTR (Fig. 5*C*). We found that low temperature and corrector C18 additively enhanced Band C % of ΔF508/AG-CFTR (Fig. 5*C*), similar to that in ΔF508-CFTR (Fig. 3*C*). Because of a greatly improved Band C % of ΔF508/AG-CFTR (Fig. 5*A*), the

enhancement (Fig. 5*C*) or fold increase (Fig. 5*D*) in Band C % of ΔF508/AG-CFTR by two different rescue methods was much lower than that of ΔF508-CFTR ($P<0.05$, Fig. 3*C*, 5*D*). Of note, the combination treatment enhanced Band C % of ΔF508/AG-CFTR to about 91% (Fig. 5*C*), close to that of wild-type CFTR (~ 96%) (Fig. 5*A*). These data suggest that G509A/V510G mutations together with low temperature and corrector C18 rescued most processing defects of ΔF508-CFTR.

Like ΔY512-CFTR, ΔY512/2A-CFTR also showed a large increase in Band C % with corrector C18 (Fig. 5*C*). The fold increases in Band C % by corrector C18 in these two mutants were similar (black columns, Fig. 5*D*). However, low temperature strikingly promoted Band C % of ΔY512/2A-CFTR (Fig. 5*C*) and the fold increase in Band C % (Fig. 5*D*) to about 69% and 9.0-fold, respectively, larger than about 50% and 4.4-fold in ΔY512-CFTR ($P<0.05$, Fig. 3*C*, 5*D*). Moreover, corrector C18 at 27 ºC only showed a small synergistic increase in Band C % of ΔY512/2A-CFTR (Fig. 5*C*), similar to that of ΔY512-CFTR (Fig. 3*C*). Therefore, these data suggest that removing side chains of V510 and S511 from ΔY512-CFTR magnified the low temperature-mediated correction of the protein processing defect. All data support our hypothesis, suggesting that residue properties of the H3-H4 loop are associated with the rescue effect of low temperature and corrector C18 on ΔF508- and ΔY512-CFTR processing.

Next, we asked whether the gating defect of ΔF508- and ΔY512-CFTR could be alleviated by loop mutations.

IBI prolongation of ΔF508- and ΔY512-CFTR is attenuated by loop mutations

When compared to wild-type CFTR, ΔF508/AG- and ΔY512/2A-CFTR showed no alterations in the single-channel current amplitude (i) and MBD (Fig. 6*A*, *B*, *D*). However, the P_o of ΔF508/AG- and ΔY512/2A-CFTR were moderately decreased (Fig. 6*C*) due to an approximately 2-fold prolongation of IBI (Fig. 6*E*). Importantly, the IBI of ΔF508/AG- and ΔY512/2A-CFTR (Fig. 6*E*) were shorter than those of ΔF508- and ΔY512-CFTR, respectively ($P<0.05$ for both mutants, Fig. 4*E*). As a result, the channel activity (Fig. 6*A*) and P_o (Fig. 6*C*) of ΔF508/AG- and ΔY512/2A-CFTR appeared greater than those of ΔF508- and ΔY512-CFTR, respectively (Fig. 4*A*, *C*; $P<0.05$ for P_o for both mutants). Because G509A/V510G mutations strikingly rescued ΔF508-CFTR processing and gating, the data suggest that they are revertant mutations similar to those described previously (e.g., 46-51). These data further suggest that displacement of the G509 residue in the H3-H4 loop may be a pivotal defect that underlies functional abnormalities of ΔF508-CFTR.

We next asked whether the rescue effects of G509A/V510G mutations may be associated with alterations in the structure and dynamics of NBD1. The crystal structure of ΔF508/AG NBD1 was modeled from ΔF508 NBD1 (PDB: 2PZF) and then subjected to replica-exchange molecular dynamics (REMD) simulation (Fig. 7*A*) and the secondary structure analysis (Fig. 7*B*, Table 1).

G509A/V510G mutations enhance protein stability of ΔF508 NBD1 and persistence of the H3 helix

Figure 7*A* presents the profiles of the root mean square fluctuation (RMSF) obtained from three simulations of ΔF508/AG NBD1, compared to similar profiles obtained for wild-type (modeled after PDB: 2PZE) and ΔF508 NBD1 as previously described (38). The data indicate that the dynamics of residues, measured by the RMSF value, varied modestly among the three NBD1 constructs (Fig. 7*A*). Interestingly, two regions corresponding to residues 502-505 and 510-511 (vertical grey shading, Fig. 7*A*) showed consistent differences in the RMSF values across the three simulations with the order wild-type < ΔF508 < ΔF508/AG and wild-type < ΔF508/AG < ΔF508, respectively. Further analysis indicated that 25% of the residues (57 residues) in ΔF508/AG NBD1 displayed lower RMSF values than those in ΔF508 NBD1, whereas only 3% of the residues (6 residues) showed higher values. These data suggest that G509A/V510G mutations reduce the dynamics of specific residues in ΔF508 NBD1 or in other words, they enhance the structural stability of ΔF508 NBD1. Moreover, the previous study (38) has demonstrated that the protein stability of ΔF508 NBD1 is lower than that of wild-type NBD1. Therefore, we speculate that mutations G509A/V510G may rescue the functional defects of ΔF508-CFTR partly by stabilizing NBD1 structure.

To investigate the molecular basis for above alterations in protein stability of NBD1, further analysis of ΔF508/AG NBD1 revealed apparent increases in residual interactions around regions near residues 509-510. First, H-bond formation between residues 511 and 563 (Fig. S3*C*) occurred in 53% of simulations with ΔF508/AG NBD1, but only 36 % in ΔF508 NBD1. Second, H-bonds between K503 and D537 (Fig. S2*A*) and between R560 and N505 (Fig. 2*C* and S2*C*) in ΔF508/AG NBD1 were maintained across 27% and 18% of total simulations, respectively, in contrast to 17% and 8% in ΔF508 NBD1.

Since the helix is important for stabilizing the tertiary structure of the protein (52), we next analyzed the time evolution (Fig. 7*B*) and the percentage of time (%) (Table 1) in which residues 491-525 adopt specific secondary structures during the simulation of wild-type, ΔF508/AG and ΔF508 NBD1. Our data demonstrate that the helicity of the H4 helix is well maintained in all constructs throughout the simulations (Fig. 7*B*, Table 1). However, the persistence of the H3 helix formed by residues 502-507 was disrupted in ΔF508 NBD1, compared to that in wild-type NBD1 (blue color, Fig. 7*B*). This is evident by observing that almost all residues

making up this helix spent less time in an α-helix secondary structure (Table 1). In contrast, the persistence of the H3 helix in ΔF508/AG NBD1 appeared to be higher than that in ΔF508 NBD1 (Fig. 7*B*, Table 1). However, Table 1 also indicates that the length of the H3 helix in ΔF508 NBD1 was not increased upon the introduction of G509A/V510G mutations since the helicity of residue I507 was seemly reduced in this construct.

The secondary structure of the H3-H4 loop varied greatly among three constructs in residues 509-511 (Fig. 7*B*, Table 1). G509 and V510 in wild-type NBD1 mostly maintained the structure of a bend or a turn (Table 1). For ΔF508/AG NBD1, residues 509-511 spent more time in the bend structure (Table 1). For ΔF508 NBD1, only V510 frequently occupied the bend conformation, whereas G509 and S511 resided more often in the random coil structure (Table 1). These data might suggest that maintaining a bend and turn conformation for residues 509-511 is associated with structural stability required for normal CFTR function.

Taken together, these data suggest that the revertant mutation G509A/V510G might correct the ΔF508-CFTR defects partly by altering the NBD1 structure, leading to increased protein stability, persistence of the H3 helix and maintenance of bends and turns in residues 509-511 in the H3-H4 loop.

DISCUSSION

Table S1 summarizes treatments and results obtained for key CFTR mutations tested in this study. Our study revealed that side chains of N505 and D513 and the backbone of residues from the H3 helix (residues 502-508), H3-H4 loop (509-512) and H4 helix (513-524) in CFTR NBD1 (53) are structurally important for normal CFTR processing. We also found that the position of the G509 residue in the polypeptide chain is the major factor that distinguishes Band C expression between ΔF508- and ΔV510-CFTR. Data obtained for loop mutations G509A/V510G in ΔF508-CFTR and V510A/S511A in ΔY512-CFTR suggest that conformational changes of residues in the H3-H4 loop and/or persistence of the H3 helix may contribute to the processing and gating defects of ΔF508- and ΔY512-CFTR. We speculate that these local structural changes near F508 may alter the stability of the H3 helix, local peptide folding, surface topology of NBD1 and side-chain interactions.

The role of the backbone and side chain of residues near F508 in CFTR processing

It has been a question for many years how the most prevalent CF mutation ΔF508 deletes only a single residue in CFTR, but causes multiple dysfunctions. Other CF mutations at NBD1, such as ΔI507, S549I, R560T and A561E (28, 50) also severely impair Band C expression of CFTR. Recent studies suggest that the ΔF508 mutation may alter NBD1 properties by affecting its folding efficiency (13, 17, 18, 54) and folding kinetics (55,

56) with a reduced thermodynamic stability of the native state (57). The ΔF508 mutation also impairs CFTR assembly (58) partly due to abnormal domain-domain interactions (14-16, 18). CFTR correctors and potentiators may rescue ΔF508-CFTR defects by targeting some of these abnormalities (23, 25, 59).

Surprisingly, most single-residue deletions near F508 in this study caused pronounced CFTR processing defects that could not be attributed to side-chain removal alone nor could they be rescued by low temperature or corrector C18. As the backbone of F508 plays a role in proper NBD1 folding (13), it is possible that abnormal folding may account for the processing defects of these deletion mutants. Following this idea, side chains of residues 503-513 mostly interact with other residues in NBD1, except that F508 and G509 also interact with ICL4 (Fig. S*2*, S*3*) (21). Moreover, since the H3-H4 loop makes a turn with residues 508-513 (Fig. 1*A* and S1*A*), deletion of residues in the middle of the loop, such as V510 and S511, may have minimal effect on folding since other residues could re-adjust their positions to compensate for the deletion (Fig. S3*B*, *C*). Our data support this hypothesis as these deletions only moderately disrupted CFTR processing (Fig. 1*B*, *C*). In contrast, deletion of residues at either end of the H3-H4 loop, including F508, G509, Y512 and D513, may significantly disrupt folding interactions (Fig. S2*F*, S3*A*, *D*, *E*) and indeed they strongly disrupted CFTR Band C expression (Fig. 1*B*, *C*).

We also found that intradomain interactions between residues N505 in the H3 helix, M498 in the Q loop and R560 in the H4 helix, contribute to structural integrity required for normal CFTR expression (Fig. 2, S2*C*). REMD simulation analysis in this study also showed that H-bond interactions between N505 and R560 in ΔF508/AG NBD1 occurred more frequently than that in ΔF508 NBD1. Recent work suggests that M498 and R560 structurally locate at the interface between NBD1 and ICL4 by the F508 residue (S2*C*) (20, 21, 60). Moreover, the exposed surface of these two residues is seemly largely extended in ΔF508-CFTR (61). Predicted by structure-based virtual screening, several novel small-molecule compounds for promoting ΔF508-CFTR expression may dock at the site containing M498 and R560 residues (62). These data suggest that interactions from the side chain of N505 may be important for NBD1 stability and could be a target for drug therapy.

G509 plays an important role in the processing defect of ΔF508-CFTR

Our data suggest that G509 shifted one position forward in the ΔF508-CFTR polypeptide chain contributes primarily to the processing defect. Our molecular analysis data (Fig. 7, Table 1) suggest that G509 in ΔF508-CFTR may destabilize the H3 helix and affect the bend and turn conformation of residues 509-511 in the H3-H4 loop. This is consistent with the well-known property of glycine as a helix breaker. Similarly, F508G-CFTR

like ΔF508-CFTR shows very little Band C expression (13, 15, 25). However, with the F508 residue unchanged, the ΔG509, but not G509A mutation profoundly reduced Band C expression of CFTR (Fig. 1*C*, 2*A*). Moreover, the F508A mutation exerted only small (Fig. 2*A*) or moderate reductions in Band C % of CFTR (13, 15, 63). The moderate Band C protein level of F508A- and G509A-CFTR suggests that when the length of the polypeptide chain remains unchanged, removing interdomain interactions from the side chain of F508 or disrupting the helix-breaker function of G509 has minor impacts on CFTR processing. Therefore, in ΔF508-CFTR, structural constraints generated by deletion of the F508 residue may be a primary cause of the defect, and together with G509 displacement greatly impair CFTR processing.

Recent studies (14, 16, 19) demonstrate that functional defects of ΔF508-CFTR are associated with abnormal interactions of NBD1 with ICL4 in MSD2, such as interactions between F508 and R1070 (Fig. S1*A*, S2*F*) (21). Restoring or enhancing these NBD1-ICL4 contacts have been shown to promote ΔF508-CFTR processing (14, 16, 19, 25, 64). Based on this mechanism, it is possible that the revertant mutation G509A/V510G-induced enhancements in the predicted stability of NBD1 and persistence of the H3 helix in ΔF508-CFTR (Fig. 7, Table 1) may facilitate NBD1-ICL4 interactions for promoting CFTR processing.

Contributions of the H3-H4 loop to the ΔF508-CFTR processing defect

Our data suggest that the H3-H4 loop in CFTR may play an important role in structural integrity required for normal protein processing and channel gating. Generally, loop structures form a connector between two rigid elements such as helices or β-sheets and works like a flexible hinge allowing for the folding of a peptide chain or like an allosteric regulator of domain-domain interactions (65). CFTR cryo-EM structures (20, 21) show that the H3-H4 loop interacts mostly with other intradomain residues in NBD1 (Fig. S2, S3), except for the residues F508 and G509 which are positioned close to the R1070 residue (Fig. S2*F*, S3*A*). Although it is unclear whether this loop exhibits dynamic and multiple conformations in native CFTR for domain-domain interactions, our data suggest that neither removing interactions from each residue's side chain nor increasing loop flexibility by glycine substitutions altered Band C expression of wild-type CFTR (Fig. 2*A*, 5*A*).

By contrast, residue deletions in the loop displayed varying impacts on Band C % of CFTR (Fig. 1*B*, *C*). Because this loop turns the H3 and H4 helices to face each other for chelating the H5 helix in NBD1 (Fig. 2*C*, S1*A*), these data suggest that the loop-mediated helix-turn-helix structure, possibly affected by deletion-induced constraints, may be an important factor regulating CFTR processing. Consistently, our data indicate that the bend and turn secondary structures of residues 509-511 seemly occurred more frequently in wild-type and ΔF508/AG NBD1 than that in ΔF508 NBD1 (Fig. 7*B*, Table 1). Moreover, residues 502-524 covering the

H3 helix, loop and H4 helix are highly conserved in CFTR among different species (Fig. S4). Key residues for maintaining normal CFTR processing such as N505, F508, G509, Y512 and D513 are also highly conserved in these CFTR orthologues (Fig. S4). These data may reveal the importance of theses residues in structural integrity required for normal CFTR function.

Our data indicate that structural changes of residues in the shortened loop were associated with the low temperature-rescued processing defect in ΔF508- and ΔY512-CFTR. Low temperature may facilitate CFTR thermodynamic folding and enhance thermal stability (17, 23, 24, 54, 56, 57, 66-69), suggesting that protein stability of NBD1 may be associated with the functional defects of ΔF508-CFTR. Similarly, the revertant mutation G509A/V510G enhanced the predicted protein stability of ΔF508 NBD1 (Fig. 7*A*). Previous work using REMD simulations (38) demonstrates that the dynamics of some residues in the H3 and H5 helices were different between wild-type and ΔF508 NBD1 (Fig. 7*A*). Interestingly, several second-site revertant mutations that improve ΔF508-CFTR processing are found in the H5 helix, such as G550E, R553M, and R555K (46, 47, 50, 63, 70). Some of these mutations also increase both the protein (38) and thermal (57) stability of ΔF508 NBD1. Therefore, these data suggest that NBD1 instability may be associated with the ΔF508-CFTR defects.

Our study demonstrates that Band C expression of CFTR was largely reduced by all deletion mutations in H3 and H4 (Fig. 1) or by site-directed mutations at N505 and R560 residues in H3 and H5 helices, respectively (Fig. 2). Similarly, trivial Band C expression is observed in the CF mutant R560T- (30, 50, 71) and R560S-CFTR (72). Taken together, our own and previous data highlight the importance of H3, H4 and H5 helices in achieving normal CFTR processing. We speculate that loop mutations and other mutations near F508 may disturb the alignment of these three helices, resulting in abnormal NBD1 folding and stability, which could be recognized as a structural defect by quality control mechanisms in the ER (4), targeting CFTR for degradation.

Revertant mutations of the loop partially correct the CFTR gating defect

The gating defect of ΔF508-CFTR is characterized by a slow channel opening rate, which is shown as prolonged IBI in CFTR gating kinetics (Fig. 4*E*) (6-8). The channel opening rate of ΔF508-CFTR can be markedly enhanced by introducing revertant mutations near ATP binding sites (50), by mutations at domain-domain interfaces between NBD1 and MSD1, MSD2 or NBD2 (14, 16, 19, 73) or by adding potentiators to stimulate ATP-dependent CFTR gating (7, 74). Interestingly, those revertant mutations that correct domain-domain interactions between NBD1 and other regions in CFTR such as R1070W in ICL4 (14, 73) or that may affect ATP function in two NBDs such as G550E (50) all greatly stimulate the channel activity of ΔF508-CFTR,

but show little or no effects on CFTR processing (14, 16, 19, 50, 73). These data may suggest that the processing and gating defect of ΔF508-CFTR are generated by different mechanisms (19).

However, in this study loop mutations G509A/V510G greatly enhanced both the Band C expression (Fig. 5*A*) and channel activity of ΔF508-CFTR (Fig. 6*A*). Similarly, V510A/S511A mutations greatly enhanced the rescue effect of low temperature on protein processing of ΔY512-CFTR (Fig. 5*C*) and partially corrected its gating defect (Fig. 6*E*). Our data suggest that deletion of a residue and displacement of the G509 residue in the H3-H4 loop form pivotal defects of ΔF508-CFTR, possibly further inducing structural abnormalities that separately lead to either the processing or channel gating defect.

In conclusion, this study characterized the role of residues near F508 in CFTR processing. Our data suggest that abnormalities of the H3 helix and the H3-H4 loop may impair CFTR processing and gating, and contribute to dysfunction of ΔF508-CFTR. We also found that low temperature and corrector C18 stimulated protein expression of not only ΔF508-CFTR but also some other CFTR deletion mutants that miss a residue in the H3-H4 loop. Therefore, even if drug cocktails of CFTR correctors and potentiators provide a promising cure for people with CF (75), our data highlight the possibility that small molecules, which correct defects in the H3 helix and H3-H4 loop might rescue both the processing and gating defects of ΔF508-CFTR.

ACKNOWLEDGEMENTS

We thank Professor Michael J. Welsh for generous gifts of wild-type human CFTR plasmids, Professor Robert J. Bridges, Rosalind Franklin University of Medicine and Science, and Cystic Fibrosis Foundation Therapeutics for providing the CFTR correctors and our departmental colleagues for valuable discussions. We acknowledge SM Chan for his great assistance with our experiments. This work was supported by grants from the Hong Kong Research Grant Council (ECS#HKU 789713M and GRF#17106315) and National Natural Science Foundation of China (NSFC#31370765 and #81570001) to JHC. This work was also supported by grants from the Cystic Fibrosis Foundation Therapeutics (SENDER13XX0) and Binational Science Foundation (2013391) to HS. In addition, XC, SZ and WX were recipients of postgraduate scholarships from the University of Hong Kong. WX was also a recipient of Lee Shau Kee Postgraduate Fellowship at the University of Hong Kong. SJB was the recipient of an Industrial CASE studentship from the Medical Research Council (grant no. MR/L015919/1).

Author contributions

H.S. and J.H.C. designed research; X.C., S.Z., M.Z., W.X., M.P.F.W. and J.H.C. performed research; G.P.H.L., H.S. and J.H.C. contributed to conception or analytic tools; X.C., S.Z., M.Z., W.X., S.J.B. and J.H.C. analyzed data; M.Z., H.S. and J.H.C. wrote the paper.

REFERENCES

1. Riordan, J. R., Rommens, J. M., Kerem, B., Alon, N., Rozmahel, R., Grzelczak, Z., Zielenski, J., Lok, S., Plavsic, N., Chou, J. L., Drumm, M. L., Iannuzzi, M. C., Collins, F. S., and Tsui, L. C. (1989) Identification of the cystic fibrosis gene: cloning and characterization of complementary DNA. *Science* **245**, 1066-1073
2. Welsh, M. J. (2010) Targeting the basic defect in cystic fibrosis. *N. Engl. J. Med.* **363**, 2056-2057
3. Hwang, T. C., and Kirk, K. L. (2013) The CFTR ion channel: gating, regulation, and anion permeation. *Cold Spring Harb. Perspect. Med.* **3**, a009498
4. Amaral, M. D., and Farinha, C. M. (2013) Rescuing mutant CFTR: a multi-task approach to a better outcome in treating cystic fibrosis. *Curr. Pharm. Des.* **19**, 3497-3508
5. Okiyoneda, T., Barriere, H., Bagdany, M., Rabeh, W. M., Du, K., Hohfeld, J., Young, J. C., and Lukacs, G. L. (2010) Peripheral protein quality control removes unfolded CFTR from the plasma membrane. *Science* **329**, 805-810
6. Hwang, T. C., Wang, F., Yang, I. C., and Reenstra, W. W. (1997) Genistein potentiates wild-type and ΔF508-CFTR channel activity. *Am. J. Physiol.* **273**, C988-998
7. Cai, Z., and Sheppard, D. N. (2002) Phloxine B interacts with the cystic fibrosis transmembrane conductance regulator at multiple sites to modulate channel activity. *J. Biol. Chem.* **277**, 19546-19553
8. Dalemans, W., Barbry, P., Champigny, G., Jallat, S., Dott, K., Dreyer, D., Crystal, R. G., Pavirani, A., Lecocq, J.-P., and Lazdunski, M. (1991) Altered chloride ion channel kinetics associated with the ΔF508-cystic fibrosis mutation. *Nature* **354**, 526-528
9. Ostedgaard, L. S., Rogers, C. S., Dong, Q., Randak, C. O., Vermeer, D. W., Rokhlina, T., Karp, P. H., and Welsh, M. J. (2007) Processing and function of CFTR-ΔF508 are species-dependent. *Proc. Natl. Acad. Sci. U. S. A.* **104**, 15370-15375
10. Drumm, M. L., Wilkinson, D. J., Smit, L. S., Worrell, R. T., Strong, T. V., Frizzell, R. A., Dawson, D. C., and Collins, F. S. (1991) Chloride conductance expressed by ΔF508 and other mutant CFTRs in Xenopus oocytes. *Science* **254**, 1797-1799
11. Wang, F., Zeltwanger, S., Hu, S., and Hwang, T. C. (2000) Deletion of phenylalanine 508 causes attenuated phosphorylation-dependent activation of CFTR chloride channels. *J. Physiol.* **524**, 637-648
12. Ostedgaard, L. S., Meyerholz, D. K., Chen, J. H., Pezzulo, A. A., Karp, P. H., Rokhlina, T., Ernst, S. E., Hanfland, R. A., Reznikov, L. R., Ludwig, P. S., Rogan, M. P., Davis, G. J., Dohrn, C. L., Wohlford-Lenane, C., Taft, P. J., Rector, M. V., Hornick, E., Nassar, B. S., Samuel, M., Zhang, Y., Richter, S. S., Uc, A., Shilyansky, J., Prather, R. S., McCray, P. B., Jr., Zabner, J., Welsh, M. J., and Stoltz, D. A.

(2011) The ΔF508 mutation causes CFTR misprocessing and cystic fibrosis-like disease in pigs. *Sci. Transl. Med.* **3**, 74ra24

13. Thibodeau, P. H., Brautigam, C. A., Machius, M., and Thomas, P. J. (2005) Side chain and backbone contributions of Phe508 to CFTR folding. *Nat. Struct. Biol.* **12**, 10-16
14. Rabeh, W. M., Bossard, F., Xu, H., Okiyoneda, T., Bagdany, M., Mulvihill, C. M., Du, K., di, B. S., Liu, Y., Konermann, L., Roldan, A., and Lukacs, G. L. (2012) Correction of both NBD1 energetics and domain interface is required to restore ΔF508 CFTR folding and function. *Cell* **148**, 150-163
15. Du, K., Sharma, M., and Lukacs, G. L. (2005) The ΔF508 cystic fibrosis mutation impairs domain-domain interactions and arrests post-translational folding of CFTR. *Nat. Struct. Biol.* **12**, 17-25
16. Serohijos, A. W., Hegedus, T., Aleksandrov, A. A., He, L., Cui, L., Dokholyan, N. V., and Riordan, J. R. (2008) Phenylalanine-508 mediates a cytoplasmic-membrane domain contact in the CFTR 3D structure crucial to assembly and channel function. *Proc. Natl. Acad. Sci. U. S. A.* **105**, 3256-3261
17. Qu, B. H., and Thomas, P. J. (1996) Alteration of the cystic fibrosis transmembrane conductance regulator folding pathway. *J. Biol. Chem.* **271**, 7261-7264
18. Lewis, H. A., Zhao, X., Wang, C., Sauder, J. M., Rooney, I., Noland, B. W., Lorimer, D., Kearins, M. C., Conners, K., Condon, B., Maloney, P. C., Guggino, W. B., Hunt, J. F., and Emtage, S. (2005) Impact of the ΔF508 mutation in first nucleotide-binding domain of human cystic fibrosis transmembrane conductance regulator on domain folding and structure. *J. Biol. Chem.* **280**, 1346-1353
19. Dong, Q., Ostedgaard, L. S., Rogers, C., Vermeer, D. W., Zhang, Y., and Welsh, M. J. (2012) Human-mouse cystic fibrosis transmembrane conductance regulator (CFTR) chimeras identify regions that partially rescue CFTR-ΔF508 processing and alter its gating defect. *Proc. Natl. Acad. Sci. U. S. A.* **109**, 917-922
20. Zhang, Z., and Chen, J. (2016) Atomic structure of the cystic fibrosis transmembrane conductance regulator. *Cell* **167**, 1586-1597
21. Liu, F., Zhang, Z., Csanady, L., Gadsby, D. C., and Chen, J. (2017) Molecular structure of the human CFTR ion channel. *Cell* **169**, 85-95
22. Zhang, Z., Liu, F., and Chen, J. (2017) Conformational Changes of CFTR upon Phosphorylation and ATP Binding. *Cell* **170**, 483-491
23. Meng, X., Wang, Y., Wang, X., Wrennall, J. A., Rimington, T. L., Li, H., Cai, Z., Ford, R. C., and Sheppard, D. N. (2017) Two small molecules restore stability to a subpopulation of the cystic fibrosis transmembrane conductance regulator with the predominant disease-causing mutation. *J. Biol. Chem.* **292**, 3706-3719

24. Aleksandrov, A. A., Kota, P., Aleksandrov, L. A., He, L., Jensen, T., Cui, L., Gentzsch, M., Dokholyan, N. V., and Riordan, J. R. (2010) Regulatory insertion removal restores maturation, stability and function of ΔF508 CFTR. *J. Mol. Biol.* **401**, 194-210
25. Okiyoneda, T., Veit, G., Dekkers, J. F., Bagdany, M., Soya, N., Xu, H., Roldan, A., Verkman, A. S., Kurth, M., Simon, A., Hegedus, T., Beekman, J. M., and Lukacs, G. L. (2013) Mechanism-based corrector combination restores ΔF508-CFTR folding and function. *Nat. Chem. Biol.* **9**, 444-454
26. Lewis, H. A., Wang, C., Zhao, X., Hamuro, Y., Conners, K., Kearins, M. C., Lu, F., Sauder, J. M., Molnar, K. S., Coales, S. J., Maloney, P. C., Guggino, W. B., Wetmore, D. R., Weber, P. C., and Hunt, J. F. (2010) Structure and dynamics of NBD1 from CFTR characterized using crystallography and hydrogen/deuterium exchange mass spectrometry. *J. Mol. Biol.* **396**, 406-430
27. Thomas, P. J., Shenbagamurthi, P., Sondek, J., Hullihen, J. M., and Pedersen, P. L. (1992) The cystic fibrosis transmembrane conductance regulator. Effects of the most common cystic fibrosis-causing mutation on the secondary structure and stability of a synthetic peptide. *J. Biol. Chem.* **267**, 5727-5730
28. Cheng, S. H., Gregory, R. J., Marshall, J., Paul, S., Souza, D. W., White, G. A., O'Riordan, C. R., and Smith, A. E. (1990) Defective intracellular transport and processing of CFTR is the molecular basis of most cystic fibrosis. *Cell* **63**, 827-834
29. He, L., Kota, P., Aleksandrov, A. A., Cui, L., Jensen, T., Dokholyan, N. V., and Riordan, J. R. (2013) Correctors of ΔF508 CFTR restore global conformational maturation without thermally stabilizing the mutant protein. *FASEB J.* **27**, 536-545
30. Lopes-Pacheco, M., Sabirzhanova, I., Rapino, D., Morales, M. M., Guggino, W. B., and Cebotaru, L. (2016) Correctors rescue CFTR mutations in nucleotide-binding domain 1 (NBD1) by modulating proteostasis. *Chembiochem* **17**, 493-505
31. Luz, S., Kongsuphol, P., Mendes, A. I., Romeiras, F., Sousa, M., Schreiber, R., Matos, P., Jordan, P., Mehta, A., Amaral, M. D., Kunzelmann, K., and Farinha, C. M. (2011) Contribution of casein kinase 2 and spleen tyrosine kinase to CFTR trafficking and protein kinase A-induced activity. *Mol. Cell. Biol.* **31**, 4392-4404
32. Pissarra, L. S., Farinha, C. M., Xu, Z., Schmidt, A., Thibodeau, P. H., Cai, Z., Thomas, P. J., Sheppard, D. N., and Amaral, M. D. (2008) Solubilizing mutations used to crystallize one CFTR domain attenuate the trafficking and channel defects caused by the major cystic fibrosis mutation. *Chem. Biol.* **15**, 62-69
33. Atwell, S., Brouillette, C. G., Conners, K., Emtage, S., Gheyi, T., Guggino, W. B., Hendle, J., Hunt, J. F., Lewis, H. A., Lu, F., Protasevich, I. I., Rodgers, L. A., Romero, R., Wasserman, S. R., Weber, P. C., Wetmore, D., Zhang, F. F., and Zhao, X. (2010) Structures of a minimal human CFTR first nucleotide-

binding domain as a monomer, head-to-tail homodimer, and pathogenic mutant. *Protein Eng. Des. Sel.* **23**, 375-384

34. Chen, J. H., Xu, W., and Sheppard, D. N. (2017) Altering intracellular pH reveals the kinetic basis of intraburst gating in the CFTR Cl^- channel. *J. Physiol.* **595**, 1059-1076
35. Carson, M. R., Travis, S. M., and Welsh, M. J. (1995) The two nucleotide-binding domains of cystic fibrosis transmembrane conductance regulator (CFTR) have distinct functions in controlling channel activity. *J. Biol. Chem.* **270**, 1711-1717
36. Venglarik, C. J., Schultz, B. D., Frizzell, R. A., and Bridges, R. J. (1994) ATP alters current fluctuations of cystic fibrosis transmembrane conductance regulator: evidence for a three-state activation mechanism. *J. Gen. Physiol.* **104**, 123-146
37. Dassault Systèmes BIOVIA. Discovery Studio Modeling Environment; Release 2017; Dassault Systèmes: San Diego: Dassault Systèmes, 2016.
38. Zhenin, M., Noy, E., and Senderowitz, H. (2015) REMD simulations reveal the dynamic profile and mechanism of action of deleterious, rescuing, and stabilizing perturbations to NBD1 from CFTR. *J Chem. Inf. Model* **55**, 2349-2364
39. Kanelis, V., Hudson, R. P., Thibodeau, P. H., Thomas, P. J., and Forman-Kay, J. D. (2010) NMR evidence for differential phosphorylation-dependent interactions in WT and ΔF508 CFTR. *EMBO J.* **29**, 263-277
40. Denning, G. M., Anderson, M. P., Amara, J. F., Marshall, J., Smith, A. E., and Welsh, M. J. (1992) Processing of mutant cystic fibrosis transmembrane conductance regulator is temperature-sensitive. *Nature* **358**, 761-764
41. Pedemonte, N., Lukacs, G. L., Du, K., Caci, E., Zegarra-Moran, O., Galietta, L. J., and Verkman, A. S. (2005) Small-molecule correctors of defective ΔF508-CFTR cellular processing identified by high-throughput screening. *J. Clin. Invest.* **115**, 2564-2571
42. Vauthier, V., Housset, C., and Falguieres, T. (2017) Targeted pharmacotherapies for defective ABC transporters. *Biochem. Pharmacol.* **136**, 1-11
43. Bebok, Z., Venglarik, C. J., Panczel, Z., Jilling, T., Kirk, K. L., and Sorscher, E. J. (1998) Activation of ΔF508 CFTR in an epithelial monolayer. *Am. J. Physiol.* **275**, C599-C607
44. Wang, Y., Liu, J., Loizidou, A., Bugeja, L. A., Warner, R., Hawley, B. R., Cai, Z., Toye, A. M., Sheppard, D. N., and Li, H. (2014) CFTR potentiators partially restore channel function to A561E-CFTR, a cystic fibrosis mutant with a similar mechanism of dysfunction as F508del-CFTR. *Br. J. Pharmacol.* **171**, 4490-4503

45. Lazrak, A., Fu, L., Bali, V., Bartoszewski, R., Rab, A., Havasi, V., Keiles, S., Kappes, J., Kumar, R., Lefkowitz, E., Sorscher, E. J., Matalon, S., Collawn, J. F., and Bebok, Z. (2013) The silent codon change I507-ATC->ATT contributes to the severity of the ΔF508 CFTR channel dysfunction. *FASEB J.* **27**, 4630-4645

46. Teem, J. L., Berger, H. A., Ostedgaard, L. S., Rich, D. P., Tsui, L. C., and Welsh, M. J. (1993) Identification of revertants for the cystic fibrosis ΔF508 mutation using STE6-CFTR chimeras in yeast. *Cell* **73**, 335-346

47. DeCarvalho, A. C., Gansheroff, L. J., and Teem, J. L. (2002) Mutations in the nucleotide binding domain 1 signature motif region rescue processing and functional defects of cystic fibrosis transmembrane conductance regulator ΔF508. *J. Biol. Chem.* **277**, 35896-35905

48. Xu, Z., Pissarra, L. S., Farinha, C. M., Liu, J., Cai, Z., Thibodeau, P. H., Amaral, M. D., and Sheppard, D. N. (2014) Revertant mutants modify, but do not rescue, the gating defect of the cystic fibrosis mutant G551D-CFTR. *J. Physiol.* **592**, 1931-1947

49. Liu, J., Bihler, H., Farinha, C. M., Awatade, N. T., Romao, A. M., Mercadante, D., Cheng, Y., Musisi, I., Jantarajit, W., Wang, Y., Cai, Z., Amaral, M. D., Mense, M., and Sheppard, D. N. (2018) Partial rescue of F508del-cystic fibrosis transmembrane conductance regulator channel gating with modest improvement of protein processing, but not stability, by a dual-acting small molecule. *Br. J. Pharmacol.* **175**, 1017-1038

50. Roxo-Rosa, M., Xu, Z., Schmidt, A., Neto, M., Cai, Z., Soares, C. M., Sheppard, D. N., and Amaral, M. D. (2006) Revertant mutants G550E and 4RK rescue cystic fibrosis mutants in the first nucleotide-binding domain of CFTR by different mechanisms. *Proc. Natl. Acad. Sci. U. S. A.* **103**, 17891-17896

51. Chang, X. B., Cui, L., Hou, Y. X., Jensen, T. J., Aleksandrov, A. A., Mengos, A., and Riordan, J. R. (1999) Removal of multiple arginine-framed trafficking signals overcomes misprocessing of ΔF508 CFTR present in most patients with cystic fibrosis. *Mol.Cell* **4**, 137-142

52. Lella, M., and Mahalakshmi, R. (2017) Metamorphic proteins: emergence of dual protein folds from one primary sequence. *Biochemistry* **56**, 2971-2984

53. Lewis, H. A., Buchanan, S. G., Burley, S. K., Conners, K., Dickey, M., Dorwart, M., Fowler, R., Gao, X., Guggino, W. B., Hendrickson, W. A., Hunt, J. F., Kearins, M. C., Lorimer, D., Maloney, P. C., Post, K. W., Rajashankar, K. R., Rutter, M. E., Sauder, J. M., Shriver, S., Thibodeau, P. H., Thomas, P. J., Zhang, M., Zhao, X., and Emtage, S. (2004) Structure of nucleotide-binding domain 1 of the cystic fibrosis transmembrane conductance regulator. *EMBO J.* **23**, 282-293

54. Hoelen, H., Kleizen, B., Schmidt, A., Richardson, J., Charitou, P., Thomas, P. J., and Braakman, I. (2010) The primary folding defect and rescue of ΔF508 CFTR emerge during translation of the mutant domain. *PLoS One* **5**, e15458

55. Serohijos, A. W., Hegedus, T., Riordan, J. R., and Dokholyan, N. V. (2008) Diminished self-chaperoning activity of the ΔF508 mutant of CFTR results in protein misfolding. *PLoS. Comput. Biol.* **4**, e1000008

56. Wang, C., Protasevich, I., Yang, Z., Seehausen, D., Skalak, T., Zhao, X., Atwell, S., Spencer Emtage, J., Wetmore, D. R., Brouillette, C. G., and Hunt, J. F. (2010) Integrated biophysical studies implicate partial unfolding of NBD1 of CFTR in the molecular pathogenesis of F508del cystic fibrosis. *Protein Sci.* **19**, 1932-1947

57. Protasevich, I., Yang, Z., Wang, C., Atwell, S., Zhao, X., Emtage, S., Wetmore, D., Hunt, J. F., and Brouillette, C. G. (2010) Thermal unfolding studies show the disease causing F508del mutation in CFTR thermodynamically destabilizes nucleotide-binding domain 1. *Protein Sci.* **19**, 1917-1931

58. Rosser, M. F., Grove, D. E., Chen, L., and Cyr, D. M. (2008) Assembly and misassembly of cystic fibrosis transmembrane conductance regulator: folding defects caused by deletion of F508 occur before and after the calnexin-dependent association of membrane spanning domain (MSD) 1 and MSD2. *Mol. Biol. Cell* **19**, 4570-4579

59. Loo, T. W., and Clarke, D. M. (2017) Corrector VX-809 promotes interactions between cytoplasmic loop one and the first nucleotide-binding domain of CFTR. *Biochem. Pharmacol.* **136**, 24-31

60. Kalid, O., Mense, M., Fischman, S., Shitrit, A., Bihler, H., Ben-Zeev, E., Schutz, N., Pedemonte, N., Thomas, P. J., Bridges, R. J., Wetmore, D. R., Marantz, Y., and Senderowitz, H. (2010) Small molecule correctors of F508del-CFTR discovered by structure-based virtual screening. *J. Comput. Aided Mol. Des.* **24**, 971-991

61. Bisignano, P., and Moran, O. (2010) Molecular dynamics analysis of the wild type and dF508 mutant structures of the human CFTR-nucleotide binding domain 1. *Biochimie* **92**, 51-57

62. Odolczyk, N., Fritsch, J., Norez, C., Servel, N., da Cunha, M. F., Bitam, S., Kupniewska, A., Wiszniewski, L., Colas, J., Tarnowski, K., Tondelier, D., Roldan, A., Saussereau, E. L., Melin-Heschel, P., Wieczorek, G., Lukacs, G. L., Dadlez, M., Faure, G., Herrmann, H., Ollero, M., Becq, F., Zielenkiewicz, P., and Edelman, A. (2013) Discovery of novel potent ΔF508-CFTR correctors that target the nucleotide binding domain. *EMBO Mol. Med.* **5**, 1484-1501

63. Thibodeau, P. H., Richardson, J. M., 3rd, Wang, W., Millen, L., Watson, J., Mendoza, J. L., Du, K., Fischman, S., Senderowitz, H., Lukacs, G. L., Kirk, K., and Thomas, P. J. (2010) The cystic fibrosis-

causing mutation ΔF508 affects multiple steps in cystic fibrosis transmembrane conductance regulator biogenesis. *J. Biol. Chem.* **285**, 35825-35835

64. Loo, T. W., Bartlett, M. C., and Clarke, D. M. (2010) The V510D suppressor mutation stabilizes ΔF508-CFTR at the cell surface. *Biochemistry* **49**, 6352-6357
65. Papaleo, E., Saladino, G., Lambrughi, M., Lindorff-Larsen, K., Gervasio, F. L., and Nussinov, R. (2016) The role of protein loops and linkers in conformational dynamics and allostery. *Chem. Rev.* **116**, 6391-6423
66. Mendoza, J. L., Schmidt, A., Li, Q., Nuvaga, E., Barrett, T., Bridges, R. J., Feranchak, A. P., Brautigam, C. A., and Thomas, P. J. (2012) Requirements for efficient correction of ΔF508 CFTR revealed by analyses of evolved sequences. *Cell* **148**, 164-174
67. Wang, W., Okeyo, G. O., Tao, B., Hong, J. S., and Kirk, K. L. (2011) Thermally unstable gating of the most common cystic fibrosis mutant channel (ΔF508): "rescue" by suppressor mutations in nucleotide binding domain 1 and by constitutive mutations in the cytosolic loops. *J. Biol. Chem.* **286**, 41937-41948
68. Liu, X., O'Donnell, N., Landstrom, A., Skach, W. R., and Dawson, D. C. (2012) Thermal instability of ΔF508 cystic fibrosis transmembrane conductance regulator (CFTR) channel function: protection by single suppressor mutations and inhibiting channel activity. *Biochemistry* **51**, 5113-5124
69. Aleksandrov, A. A., Kota, P., Cui, L., Jensen, T., Alekseev, A. E., Reyes, S., He, L., Gentzsch, M., Aleksandrov, L. A., Dokholyan, N. V., and Riordan, J. R. (2012) Allosteric modulation balances thermodynamic stability and restores function of ΔF508 CFTR. *J. Mol. Biol.* **419**, 41-60
70. Teem, J. L., Carson, M. R., and Welsh, M. J. (1996) Mutation of R555 in CFTR-ΔF508 enhances function and partially corrects defective processing. *Receptors Channels* **4**, 63-72
71. He, L., Aleksandrov, L. A., Cui, L., Jensen, T. J., Nesbitt, K. L., and Riordan, J. R. (2010) Restoration of domain folding and interdomain assembly by second-site suppressors of the ΔF508 mutation in CFTR. *FASEB J.* **24**, 3103-3112
72. Awatade, N. T., Ramalho, S., Silva, I. A. L., Felicio, V., Botelho, H. M., de Poel, E., Vonk, A., Beekman, J. M., Farinha, C. M., and Amaral, M. D. (2018) R560S: A class II CFTR mutation that is not rescued by current modulators. *J Cyst Fibros* In press
73. He, L., Aleksandrov, A. A., An, J., Cui, L., Yang, Z., Brouillette, C. G., and Riordan, J. R. (2015) Restoration of NBD1 thermal stability is necessary and sufficient to correct ΔF508 CFTR folding and assembly. *J Mol Biol* **427**, 106-120
74. Jih, K. Y., and Hwang, T. C. (2013) Vx-770 potentiates CFTR function by promoting decoupling between the gating cycle and ATP hydrolysis cycle. *Proc. Natl. Acad. Sci. U. S. A.* **110**, 4404-4409

75. Guimbellot, J., Sharma, J., and Rowe, S. M. (2017) Toward inclusive therapy with CFTR modulators: Progress and challenges. *Pediatr. Pulmonol.* **52**, S4-S14

Table 1. Residence of residues 502-524 adopted specific secondary structure conformations calculated from three REMD simulations of wild-type, ΔF508/AG and ΔF508 NBD1.

H3 Helix	α-Helix			3-Helix		
Residues	WT	ΔF/AG	ΔF508	WT	ΔF/AG	ΔF508
502	60±4	58±2	42±5*	1±0	4±1*	2±1
503	71±4	64±2#	46±5*	6±1	15±1	16±4
504	85±3	67±2	54±8*	6±1	15±1	16±4
505	85±3	67±2	54±8*	6±1	13±1	16±4
506	85±2	56±1*	52±9*	0±0	0±0	0±0
507	44±6	8±2*	20±8*	0±0	0±0	0±0

H3-H4 Loop	Coil			Bend			Turn		
Residues	WT	ΔF/AG	ΔF508	WT	ΔF/AG	ΔF508	WT	ΔF/AG	ΔF508
509	0±0	35±5*#	62±3*	56±6	59±4#	21±3*	44±6	6±1*	17±5*
510	2±0	0±0	0±0	98±0	94±1	86±4*	0±0	6±1	14±4*
511	100±0	23±2*#	54±1*	0±0	77±2*#	45±1*	0±0	0±0	1±1
512	100±0	100±0	100±0	0±0	0±0	0±0	0±0	0±0	0±0
513	100±0	100±0	100±0	0±0	0±0	0±0	0±0	0±0	0±0

H4 Helix	α-Helix			3-Helix		
Residues	WT	ΔF/AG	ΔF508	WT	ΔF/AG	ΔF508
514	99±0	99±0	95±2	0±0	0±0	0±0
515	100±0	100±0	98±1	0±0	0±0	0±0
516	100±0	100±0	98±1	0±0	0±0	0±0
517	100±0	100±0	100±0	0±0	0±0	0±0
518	100±0	100±0	100±0	0±0	0±0	0±0
519	99±0	98±1	98±0	0±0	0±0	0±0
520	100±0	100±0	100±0	0±0	0±0	0±0
521	100±0	99±0	100±0	0±0	0±0	0±0
522	98±0	96±0	97±0	0±0	0±0	0±0
523	98±0	96±0*	97±0	0±0	0±0	0±0
524	10±1	9±0*#	12±0*	0±0	0±0	0±0

Data show the percentage of time (%) measured from Figure 7*B*. Data are means ± S.E.M. (N=3 for all data) for wild-type (WT), ΔF508/AG (ΔF/AG) and ΔF508 NBD1. *, $P<0.05$ vs. wild-type NBD1, one-way ANOVA. #, $P<0.05$, ΔF508/AG vs. ΔF508 NBD1, one-way ANOVA. For further details, see Figure 7.

FIGURE LEGENDS

Figure 1. Localized deletions near the F508 residue severely impair CFTR processing. *A*) Comparison of NBD1 structures between human wild-type CFTR (grey; PDB: 2BBO) and ΔF508-CFTR (green; PDB: 1XMJ). Expanded figure on the right displays the aberrant H3-H4 loop (blue) in ΔF508-NBD1 vs. the normal (grey) in wild-type NBD1. Yellow dots indicate positions of residues tested in panel B. *B, C*) Immunoblotting image (*B*) and quantitative data (*C*) show protein expression of wild-type (WT) and mutant CFTR. Columns in grey represent the data of CFTR mutants with deletions outside positions 503-513. The percentage of Band C expression ($\frac{C}{B+C}$%) was calculated by measuring protein band intensity of Band C vs. that of Bands B+C. Data are means + S.E.M. (N = 6-8). *, $P<0.05$ vs. wild-type CFTR, one-way ANOVA.

Figure 2. Side-chain function of N505 and D513 residues is required for normal CFTR processing. *A–E*) Effects of site-directed mutations on CFTR processing with alanine substitutions at residues from positions 503 to 515 (*A*) (N=6-8) and with substitutions of different residues for N505 (*B*) (N = 6-7), at N505, M498 and R560 (*C, D*) (N = 5-7) or at D513 (*E*) (N = 6-8). Data of wild-type (WT) CFTR were adapted from Figure 1*C*. Data are means + S.E.M. *, $P<0.05$ vs. wild-type CFTR, one-way ANOVA. See other details in Figure 1.

Figure 3. The processing defect of ΔY512-CFTR is rescued by low temperature and CFTR correctors. *A–D*) Band C % of wild-type (WT) CFTR or indicated mutants incubated at 27 °C (*A*), treated with the CFTR corrector C18 (10 μM) (*B*), treated with corrector C18 at 27 °C (*C*) or treated with correctors C18 and C4 (10 μM) at 27 °C (*D*). In (*A*), the control data were adapted from Figure 1*C* for each CFTR variant. The vehicle controls of 0.1% DMSO were tested at 37 °C (*B*, *C*) or at 27 °C (*D*). Data are means + S.E.M. (N = 6-10). *, $P<0.05$ vs. control, one-way ANOVA. #, $P<0.05$ between two sets of the data in ΔF508- or ΔY512-CFTR, one-way ANOVA.

Figure 4. Channel gating of ΔY512-CFTR exhibits prolonged IBI. *A*) Representative recordings show the single-channel activity of wild-type and mutant CFTR in the presence of ATP (1 mM) and PKA (75 nM). Dotted lines indicate the closed state and downward deflections correspond to channel openings. *B–E*) The single-channel current amplitude (i) (*B*), open probability (P_o) (*C*), mean burst duration (MBD) (*D*) and interburst interval (IBI) (*E*) of wild-type and mutant CFTR are shown. Data are means + S.E.M. (N = 6, except ΔF508-CFTR where N = 4). *, $P<0.05$ vs. wild-type CFTR, one-way ANOVA.

Figure 5. Differential effects of H3-H4 loop mutations on the correction of ΔF508- and ΔY512-CFTR processing. *A, B*) Effects of alanine or glycine substitutions at the H3-H4 loop on Band C % of ΔF508- (*A*) and

ΔY512-CFTR (*B*). Wild-type, ΔF508- or ΔY512-CFTR were used as controls (blank columns). In (*A*), the image of ΔF508-G509A/V510A-CFTR was acquired separately from the other data. *C*) Effects of low temperature and corrector C18 on Band C % of ΔF508/AG (G509A/V510G)-CFTR and ΔY512/2A (V510A/S511A)-CFTR. Blank columns represent the data of the vehicle control of 0.1% DMSO at 37 °C. Notably, a protein band between Band B and C was evidently found in the immunoblot of ΔF508/AG-CFTR in the presence of corrector C18, but excluded from the analysis in this and other experiments (e.g., Fig. 3*D*) due to lack of the control. *D*) The fold increase in Band C % of ΔF508-, ΔF508/AG-, ΔY512- and ΔY512/2A-CFTR by low temperature or corrector C18 vs. the control at 37 °C with no treatment (blank bars). Fold increase in Band C % = (Band C $\%_{\text{-treatment}}$) / (Band C $\%_{\text{-no treatment control at 37 °C}}$). Dotted lines indicate the fold increase in Band C % = 1 for the control. All data are means + S.E.M. (N = 6-10); *, $P<0.05$ vs. the control (blank columns), one-way ANOVA; #, $P<0.05$ between two groups, one-way ANOVA.

Figure 6. The IBI of ΔF508/AG- and ΔY512/2A-CFTR are only mildly prolonged. *A*) Representative recordings show the single-channel activity of ΔF508/AG- and ΔY512/2A-CFTR in the presence of ATP (1 mM) and PKA (75 nM). Dotted lines indicate the closed state and downward deflections correspond to channel openings. *B*–*E*) The single-channel current amplitude (i), P_o, MBD and IBI of two mutants are shown. Data are means + S.E.M. (N = 6 for both mutants). *, $P<0.05$ vs. wild-type CFTR, one-way ANOVA.

Figure 7. The revertant mutation G509A/V510G enhances protein stability and persistence of the H3 helix in ΔF508 NBD1. *A*) Three REMD simulations of wild-type (blue), ΔF508/AG (green) and ΔF508 (red) NBD1 constructs. Two vertical grey shadings indicate the RMSF values of residues 502-505 and 510-511, respectively. Data of wild-type and ΔF508 NBD1 were retrieved from the previous publication (38) with permission. *B*) Representative DSSP plots show persistence of secondary structure elements for residues 491-525 in wild-type (top), ΔF508/AG (middle) and ΔF508 (bottom) NBD1.

Figure 1

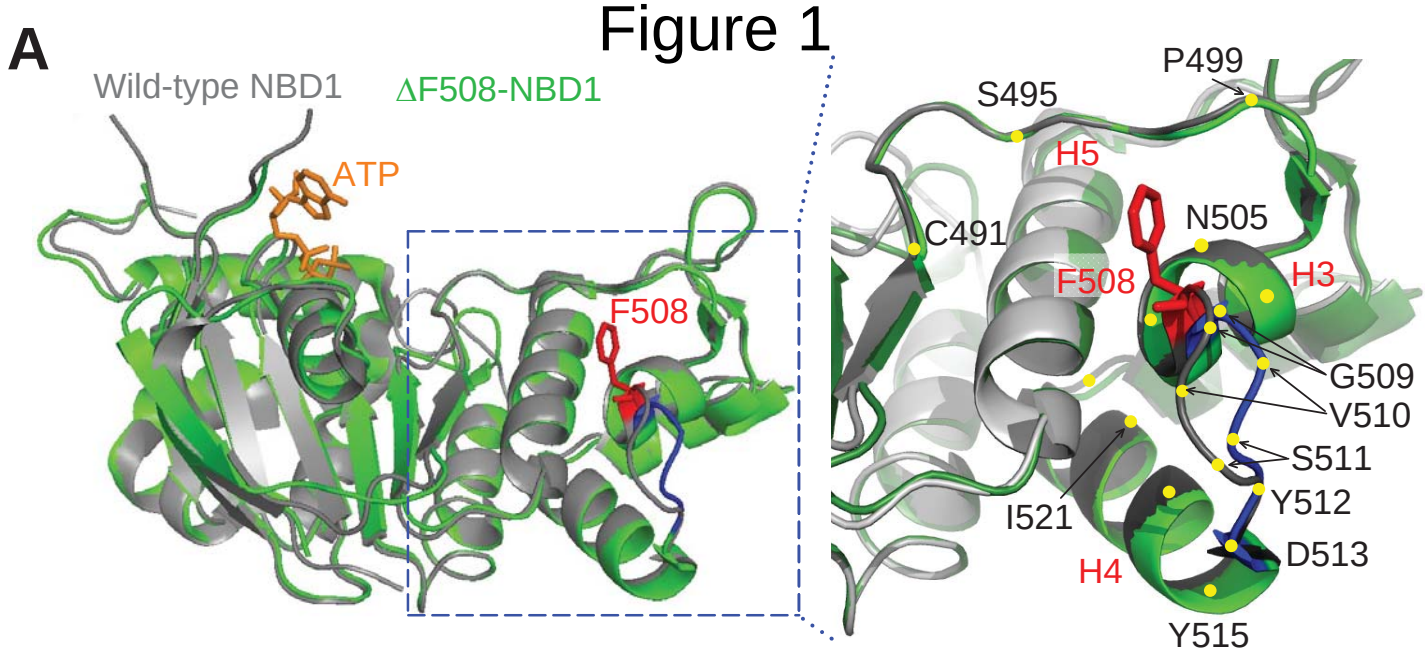
A
Wild-type NBD1
ΔF508-NBD1
ATP
F508
P499
S495
H5
C491
N505
F508
H3
G509
V510
S511
Y512
I521
H4
D513
Y515

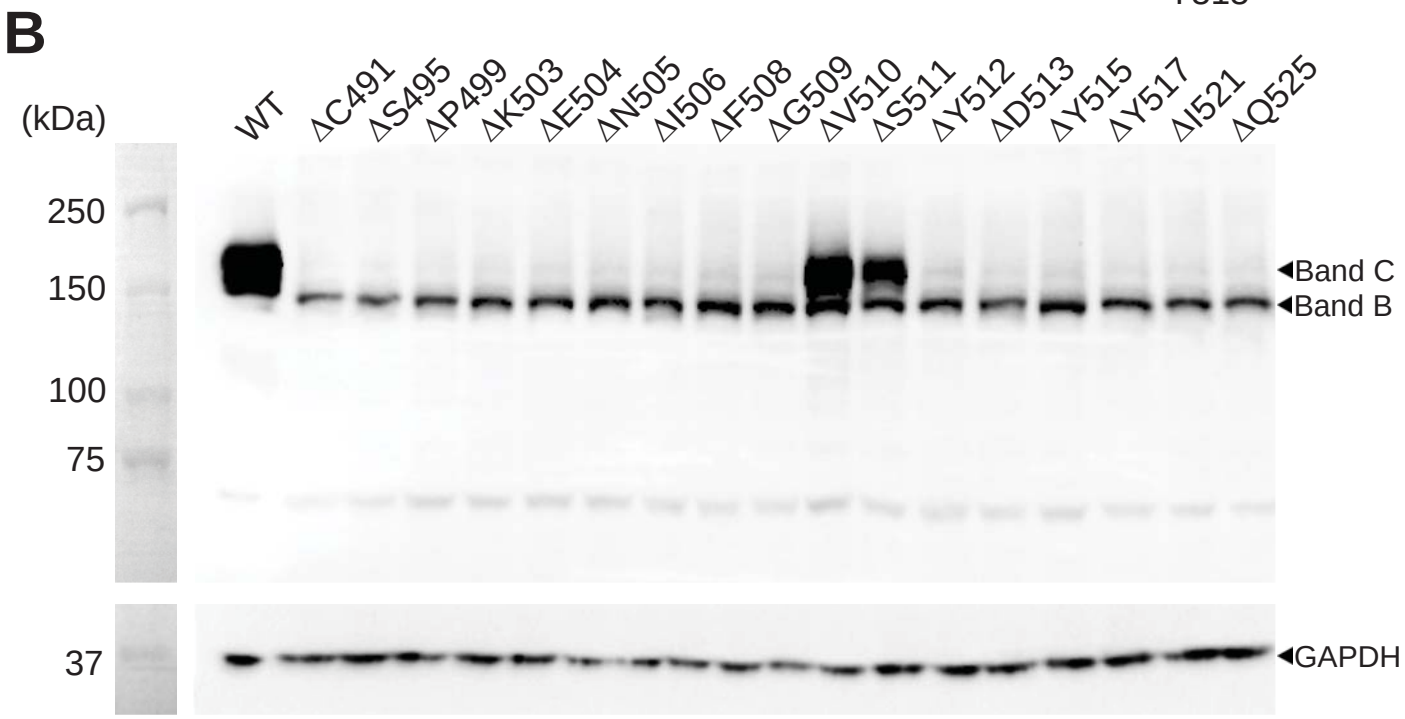
B
(kDa)
WT
ΔC491
ΔS495
ΔP499
ΔK503
ΔE504
ΔN505
ΔI506
ΔF508
ΔG509
ΔV510
ΔS511
ΔY512
ΔD513
ΔY515
ΔY517
ΔI521
ΔQ525
250
150
100
75
Band C
Band B
37
GAPDH

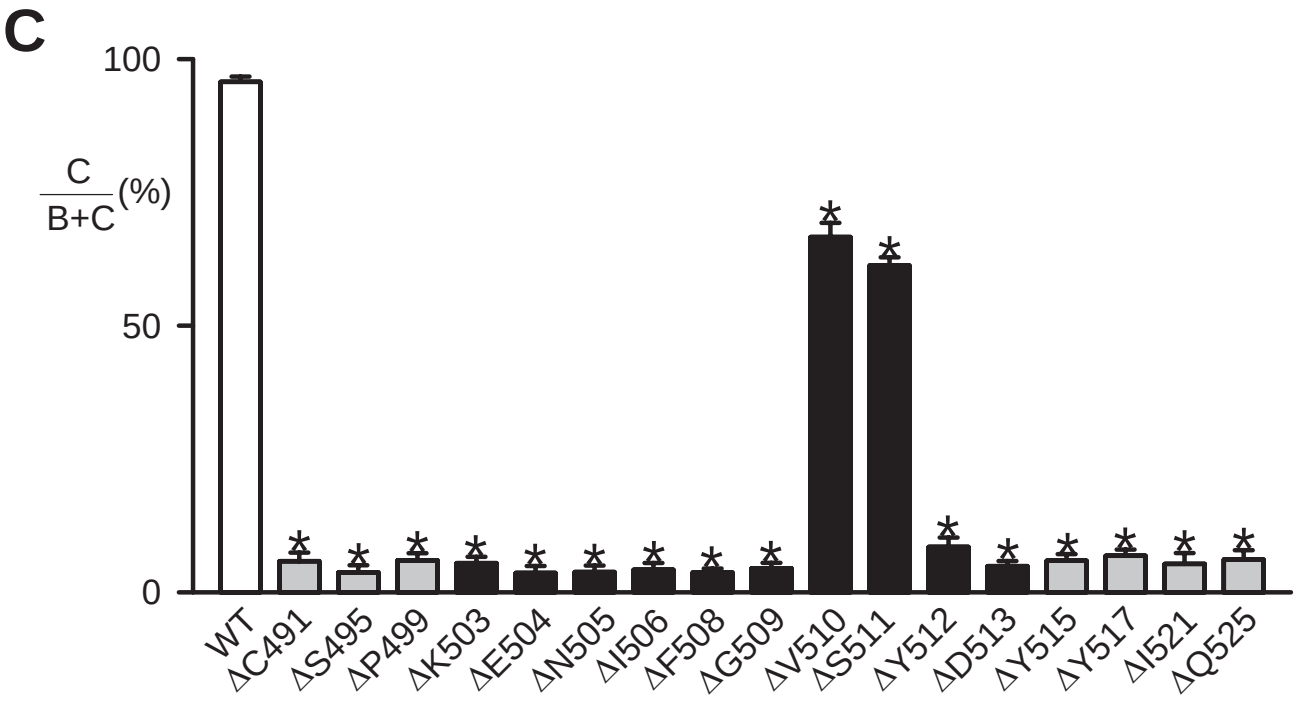
C
100
C / B+C (%)
50
0
WT
ΔC491
ΔS495
ΔP499
ΔK503
ΔE504
ΔN505
ΔI506
ΔF508
ΔG509
ΔV510
ΔS511
ΔY512
ΔD513
ΔY515
ΔY517
ΔI521
ΔQ525

Figure 2

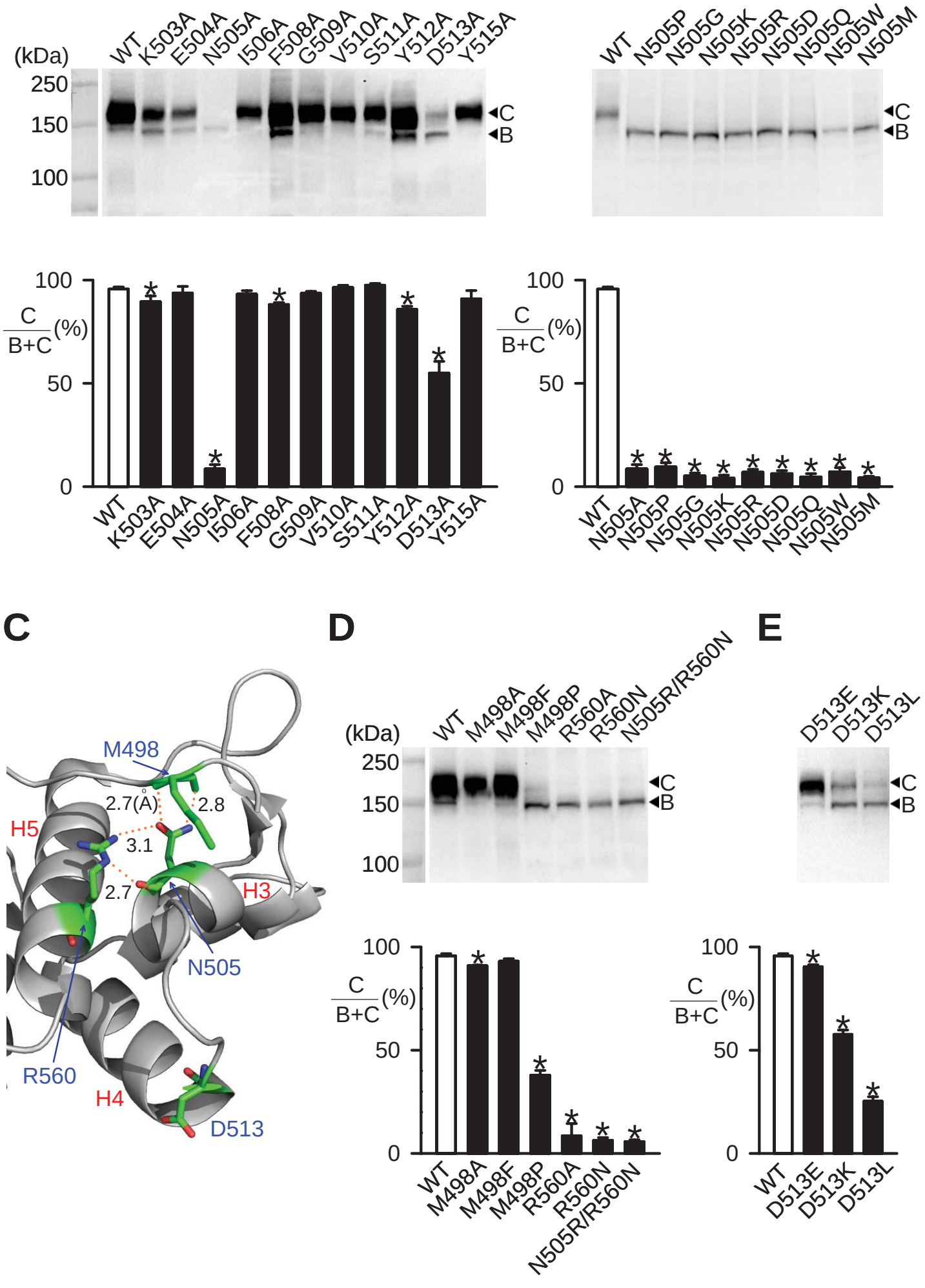
A
B
C
D
E
(kDa)
250
150
100
WT
K503A
E504A
N505A
I506A
F508A
G509A
V510A
S511A
Y512A
D513A
Y515A
N505P
N505G
N505K
N505R
N505D
N505Q
N505W
N505M
C
B
C/(B+C) (%)
50
0
M498
2.7(Å)
2.8
H5
3.1
2.7
H3
N505
R560
H4
D513
M498A
M498F
M498P
R560A
R560N
N505R/R560N
D513E
D513K
D513L

Figure 3

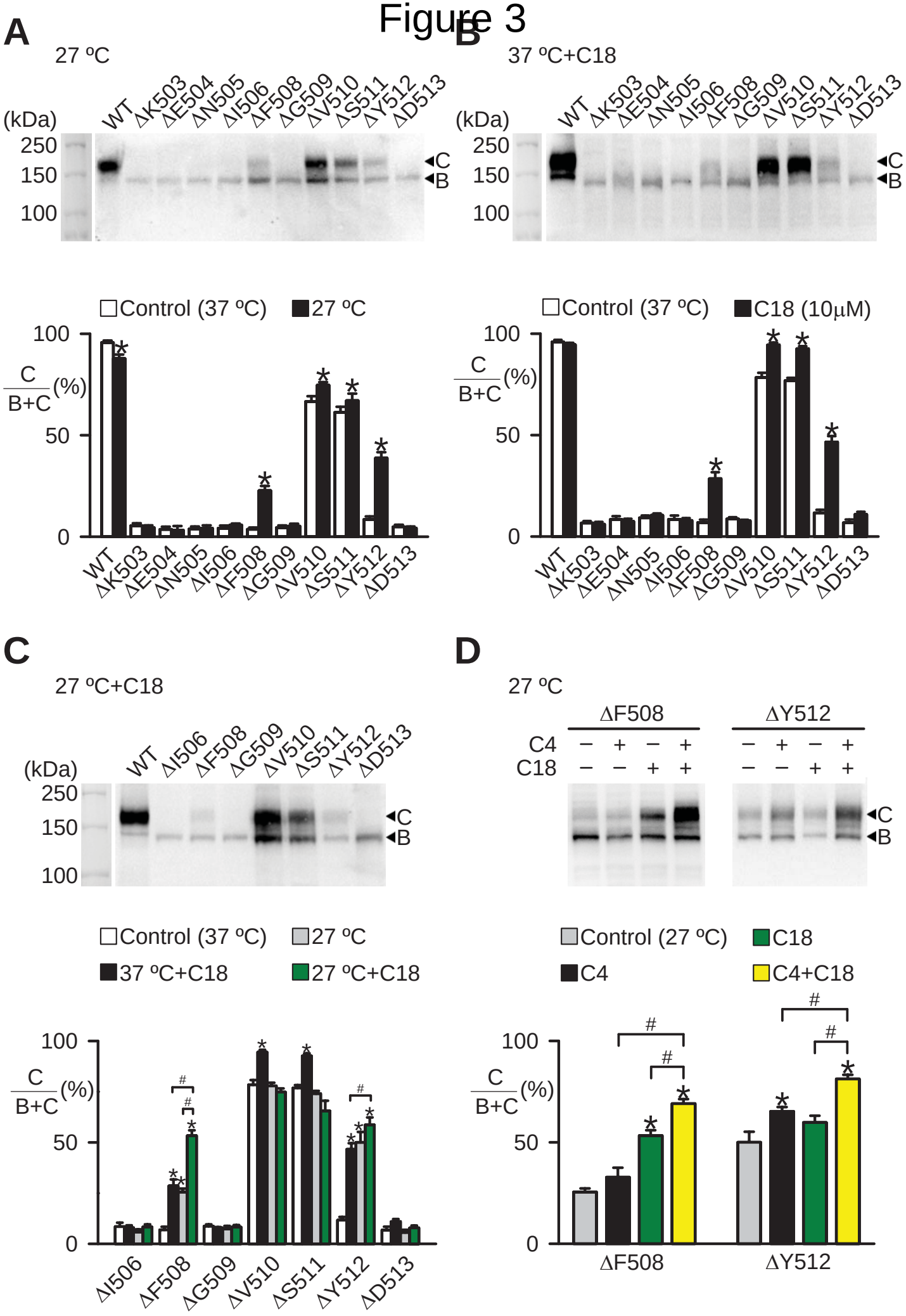
A
27 ºC
(kDa)
WT
ΔK503
ΔE504
ΔN505
ΔI506
ΔF508
ΔG509
ΔV510
ΔS511
ΔY512
ΔD513
250
150
100
C
B
Control (37 ºC)
27 ºC
C / B+C (%)
100
50
0
B
37 ºC+C18
Control (37 ºC)
C18 (10μM)
C
27 ºC+C18
Control (37 ºC)
27 ºC
37 ºC+C18
27 ºC+C18
D
27 ºC
ΔF508
ΔY512
C4
C18
Control (27 ºC)
C18
C4
C4+C18
#
*

Figure 4

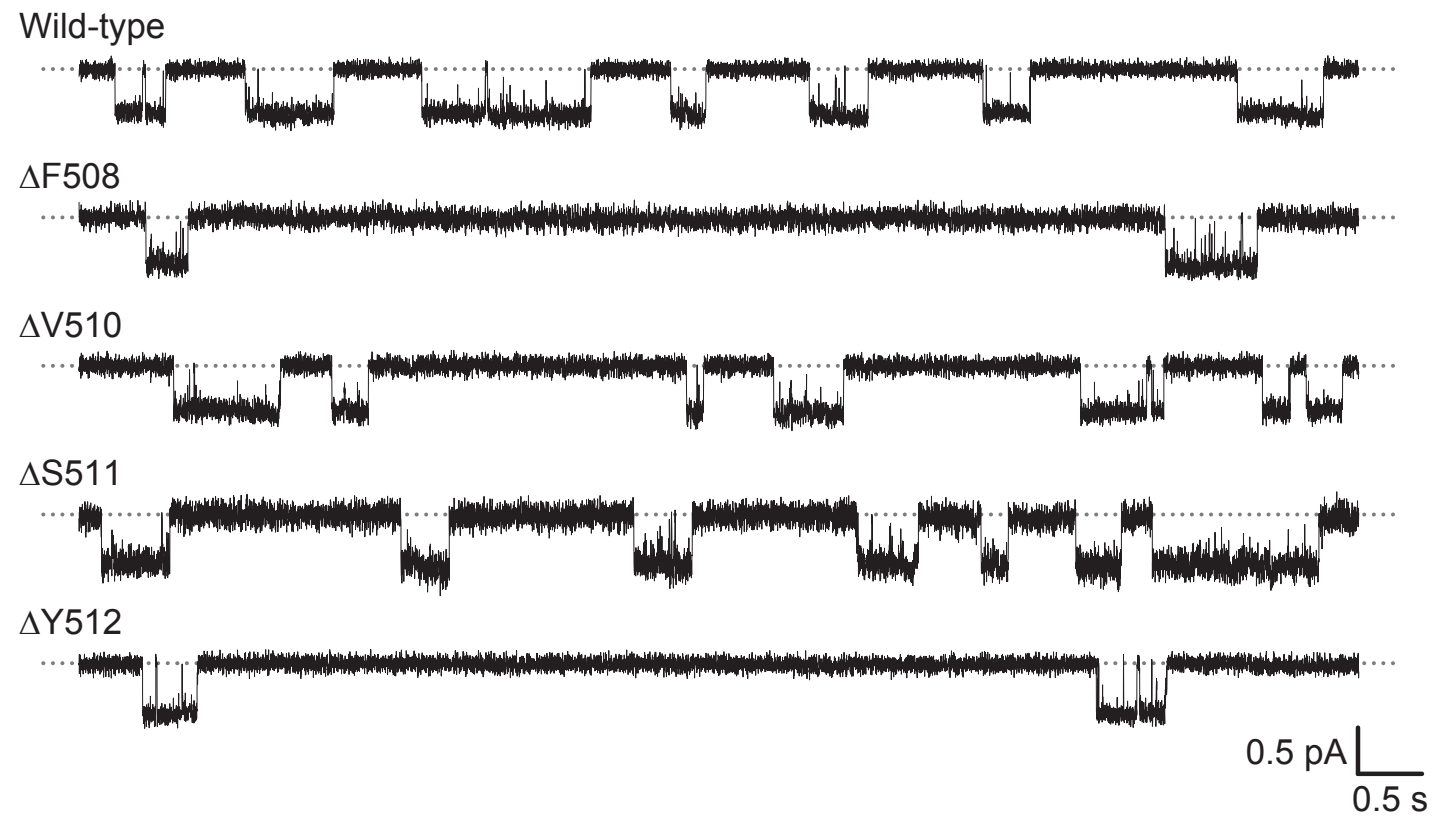
A
Wild-type
ΔF508
ΔV510
ΔS511
ΔY512
0.5 pA
0.5 s

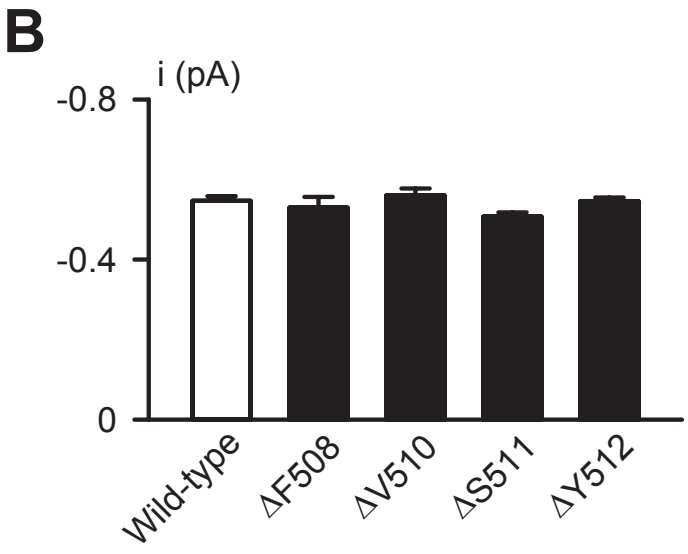
B
i (pA)
-0.8
-0.4
0
Wild-type
ΔF508
ΔV510
ΔS511
ΔY512

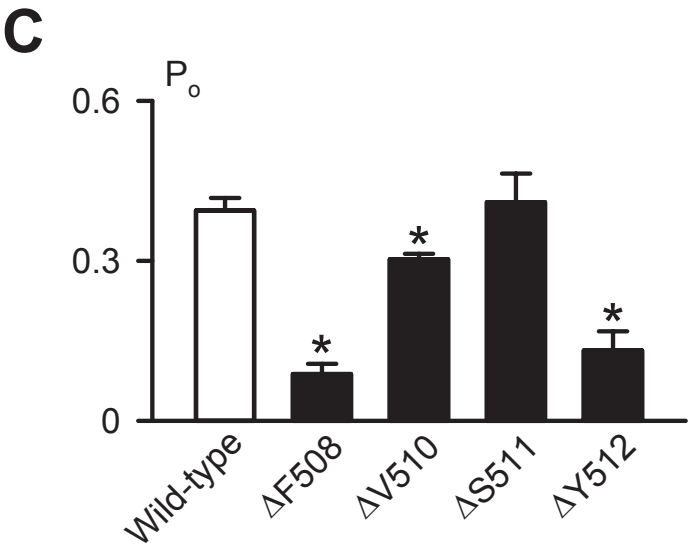
C
Po
0.6
0.3
0
*
Wild-type
ΔF508
ΔV510
ΔS511
ΔY512

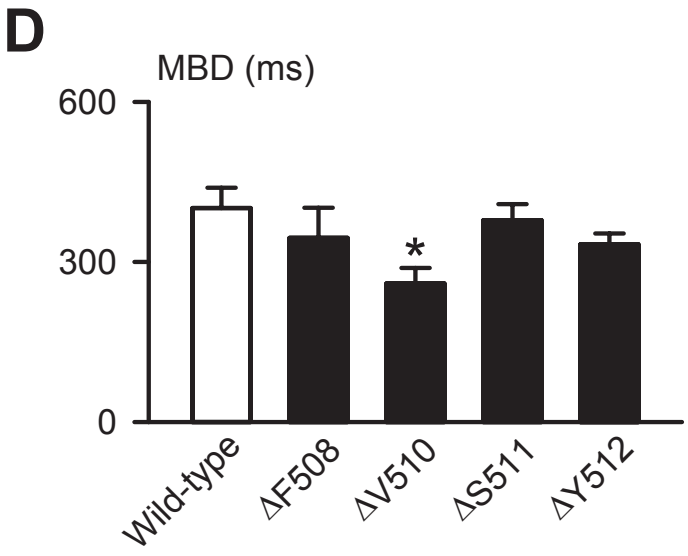
D
MBD (ms)
600
300
0
*
Wild-type
ΔF508
ΔV510
ΔS511
ΔY512

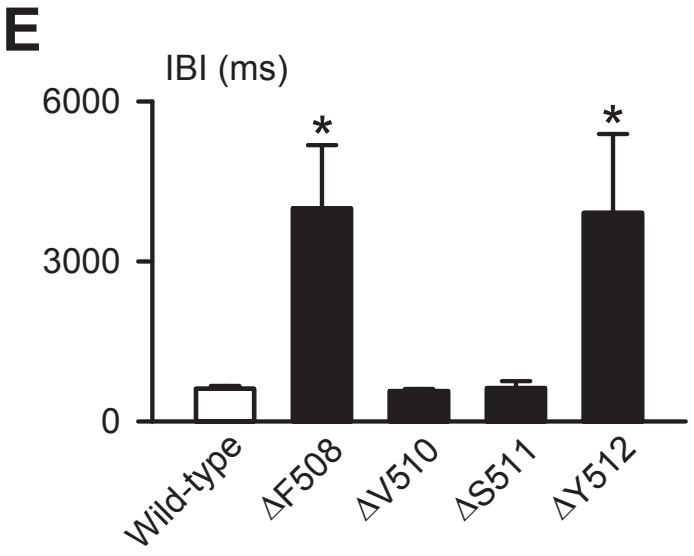
E
IBI (ms)
6000
3000
0
*
Wild-type
ΔF508
ΔV510
ΔS511
ΔY512

Figure 5

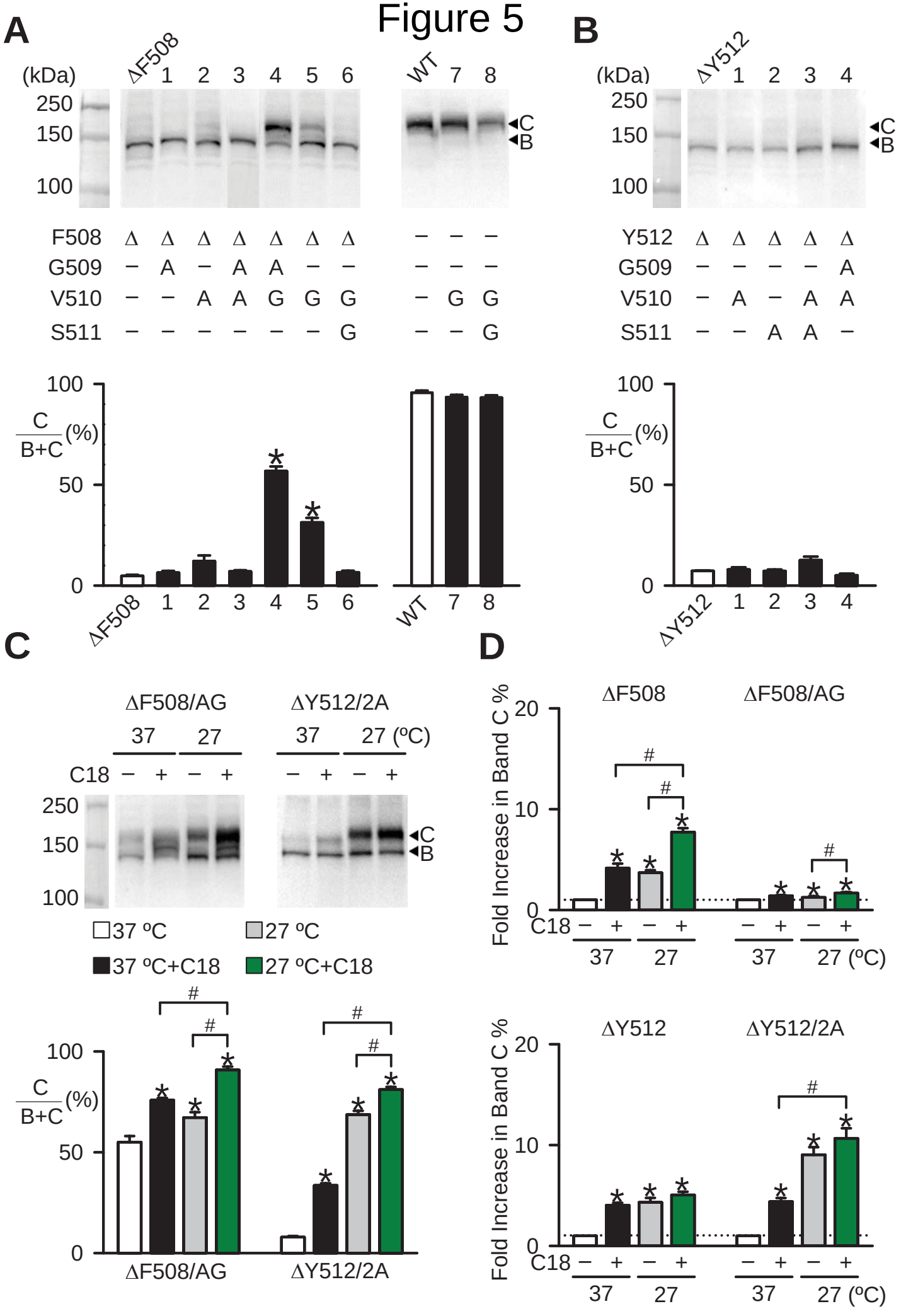
A
(kDa)
ΔF508
1 2 3 4 5 6
WT
7 8
250
150
100
C
B
F508 Δ Δ Δ Δ Δ Δ Δ – – –
G509 – A – A A – – – – –
V510 – – A A G G G – G G
S511 – – – – – – G – – G
100
C/(B+C) (%)
50
0
ΔF508 1 2 3 4 5 6 WT 7 8
B
(kDa)
ΔY512
1 2 3 4
Y512 Δ Δ Δ Δ Δ
G509 – – – – A
V510 – A – A A
S511 – – A A –
ΔY512 1 2 3 4
C
ΔF508/AG
ΔY512/2A
37 27 37 27 (ºC)
C18 – + – + – + – +
37 ºC
27 ºC
37 ºC+C18
27 ºC+C18
#
*
ΔF508/AG ΔY512/2A
D
ΔF508 ΔF508/AG
Fold Increase in Band C %
20
10
0
ΔY512 ΔY512/2A

Figure 6

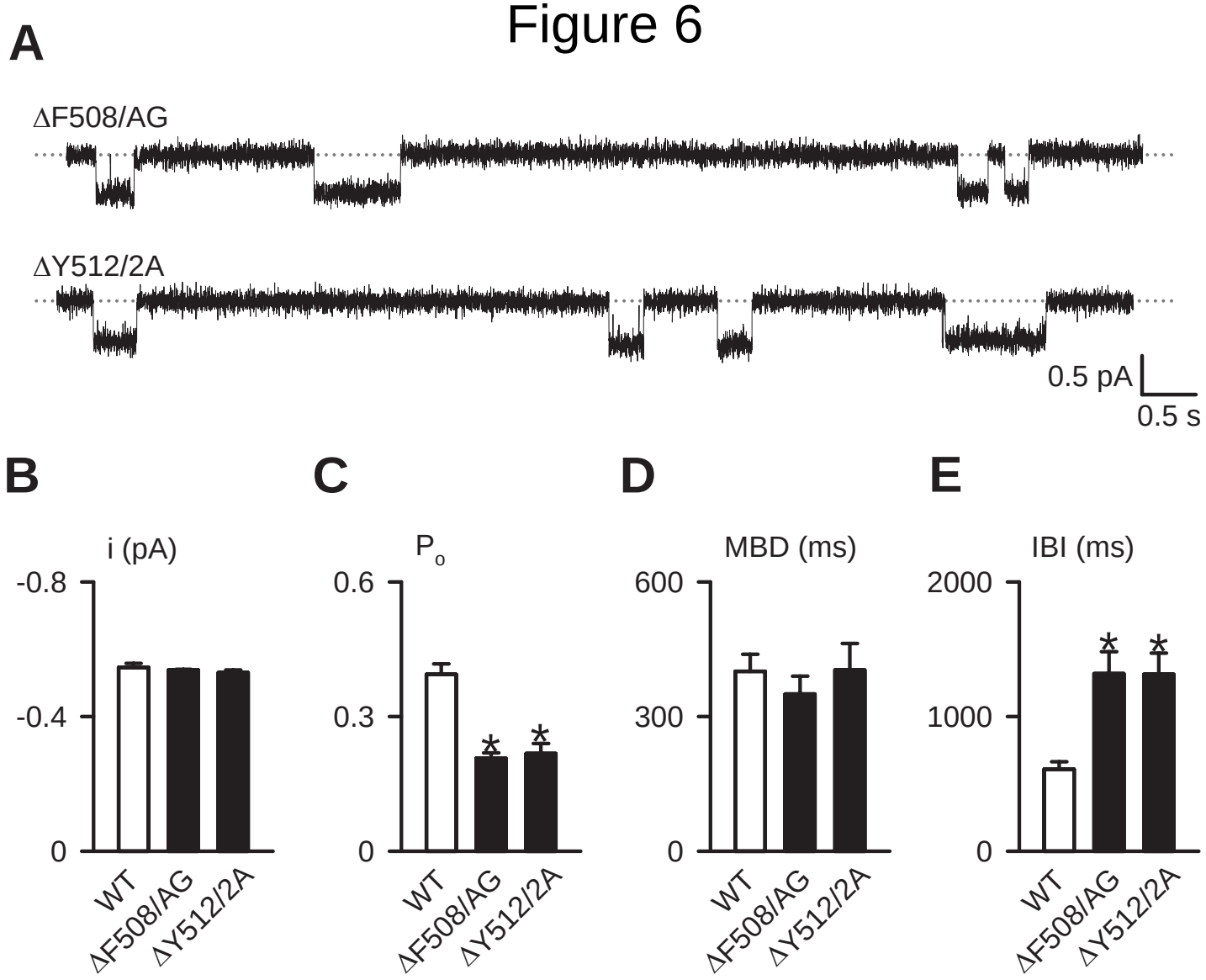
A
ΔF508/AG
ΔY512/2A
0.5 pA
0.5 s
B
i (pA)
-0.8
-0.4
0
WT
ΔF508/AG
ΔY512/2A
C
P o
0.6
0.3
0
WT
ΔF508/AG
ΔY512/2A
D
MBD (ms)
600
300
0
WT
ΔF508/AG
ΔY512/2A
E
IBI (ms)
2000
1000
0
WT
ΔF508/AG
ΔY512/2A

Figure 7

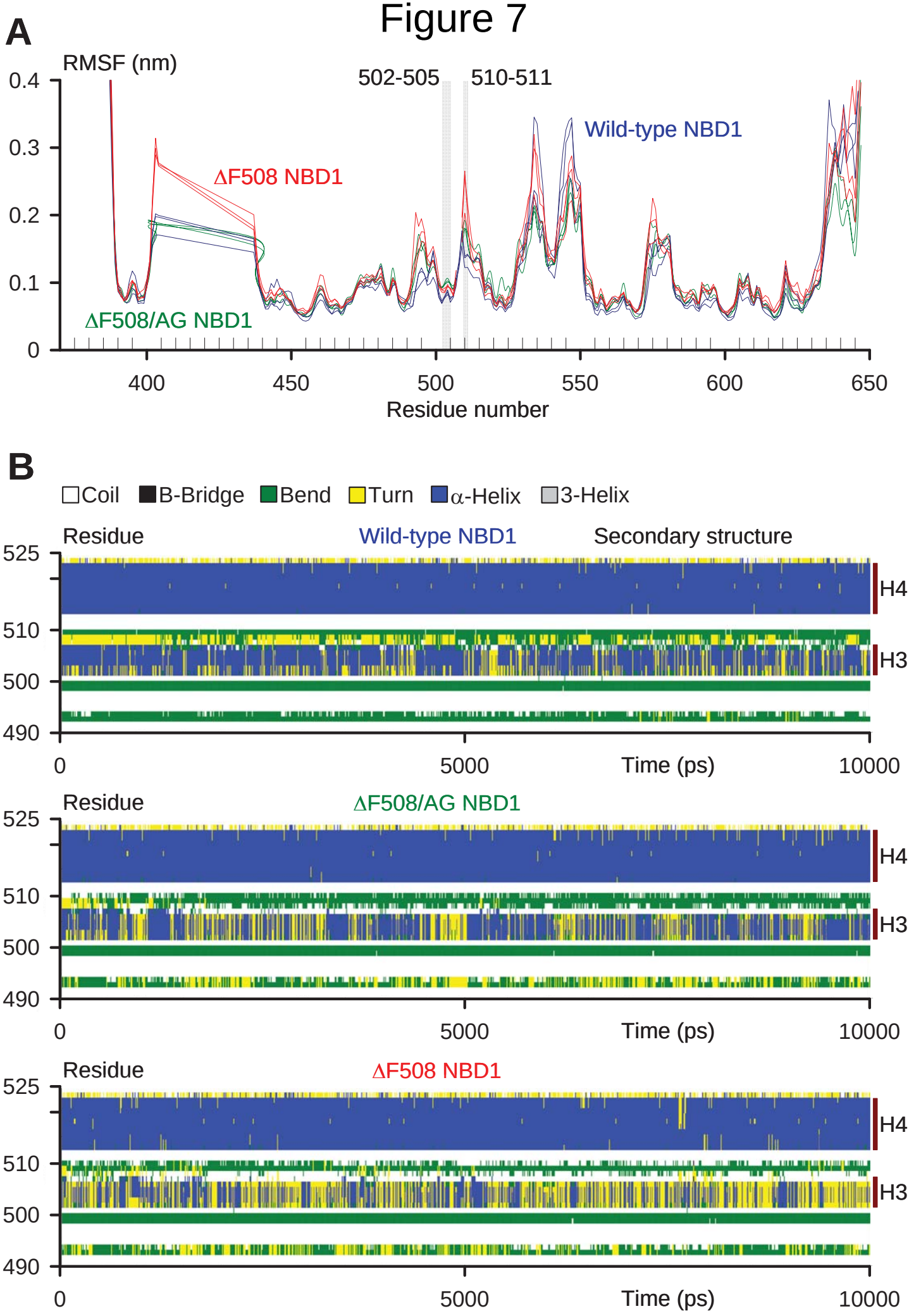
A
RMSF (nm)
0.4
0.3
0.2
0.1
0
502-505
510-511
Wild-type NBD1
ΔF508 NBD1
ΔF508/AG NBD1
400
450
500
550
600
650
Residue number
B
Coil
B-Bridge
Bend
Turn
α-Helix
3-Helix
Residue
Wild-type NBD1
Secondary structure
525
510
500
490
H4
H3
0
5000
Time (ps)
10000
Residue
ΔF508/AG NBD1
525
510
500
490
H4
H3
0
5000
Time (ps)
10000
Residue
ΔF508 NBD1
525
510
500
490
H4
H3
0
5000
Time (ps)
10000

A defective flexible loop contributes to the processing and gating defects of the predominant cystic fibrosis-causing mutation

SUPPLEMENTAL DATA

Table S1. Summary results of protein expression of key CFTR mutants tested in this study.

Residues	**K503**	**E504**	**N505**	**I506**	**I507**	**F508**	**G509**	**V510**	**S511**	**Y512**	**D513**
Alanine substitution	A	A	A	A	A	A	A	A	A	A	A
Expression scale 37°C	+++++	+++++	+	+++++	+++++	+++++	+++++	+++++	+++++	+++++	+++++
Deletion mutation	Δ	Δ	Δ	Δ		Δ	Δ	Δ	Δ	Δ	Δ
Expression scale 37°C	+	+	+	+		+	+	+++++	+++++	+	+
27°C	+	+	+	+		+++	+	+++++	+++++	++++	+
37 °C + C18	+	+	++	+		+++	+	+++++	+++++	+++++	++
27 °C + C18				+		+++++	+	+++++	+++++	+++++	++
27 °C + C4						++++				+++++	
27°C + C4 + C18						+++++				+++++	

Loop residues	**F508**	**G509**	**V510**	**S511**	**Y512**	Expression scale	*Band C %	N
ΔF508-CFTR	Δ					+	4.8 ± 0.6	6
+ G509A	Δ	A				+	6.4 ± 0.9	11
+ V510A	Δ		A			++	12.1 ± 2.9	11
+ G509A/V510A	Δ	A	A			+	7.1 ± 0.6	17
+ V510G	Δ		G			++++	31.3 ± 2.3	15
+ V510G/S511G	Δ		G	G		+	6.6 ± 0.8	11
+ G509A/V510G	Δ	A	G			+++++	56.8 ± 2.3	15
37 °C + C18	Δ	A	G			+++++	75.8 ± 1.2	6
27 °C	Δ	A	G			+++++	67.2 ± 2.7	6
27 °C + C18	Δ	A	G			+++++	90.8 ± 1.6	6

Loop residues	**F508**	**G509**	**V510**	**S511**	**Y512**	Expression scale	*Band C %	N
ΔY512-CFTR					Δ	+	7.5 ± 0.3	6
+ V510A			A		Δ	+	7.5 ± 0.7	6
+ S511A				A	Δ	+	7.2 ± 0.8	6
+ V510A/ S511A			A	A	Δ	+	8.0 ± 0.6	12
37 °C + C18			A	A	Δ	++++	33.6 ± 1.0	6
27 °C			A	A	Δ	+++++	68.7 ± 1.8	6
27 °C + C18			A	A	Δ	+++++	81.1 ± 1.3	6

Note: Expression scale is defined as follows: +, Band C % < 10%; ++, < 20%; +++, < 30%; ++++, < 40%; +++++, ≧ 40%. N indicates the number of experiments. Blank spots indicate no experiment performed. In most experiments, cells were cultured at 37 °C except where shown at 27 °C.
*, means ± S.E.M. of Band C % are shown.

SUPPLEMENTAL FIGURE LEGENDS

Figure S1. Positions of key secondary structures and residues in NBD1 tested in this study. *A*) Positions of the H3, H4 and H5 helices, F508 residue (red) and H3-H4 loop (orange) are displayed in the cryo-EM structure of human wild-type CFTR (PDB: 5UAK) with MSD1 in blue color, NBD1 in grey and MSD2 and NBD2 in green. *B, C*) Residues that interact with side chains of the D513 (B) and Y512 (C) residue are shown in NBD1 of cryo-EM human wild-type CFTR.

Figure S2. Side-chain interactions of residues 503-508 in the cryo-EM structure of human wild-type CFTR. *A-F*) Side-chain interactions of K503 (A), E504 (B), N505 (C), I506 (D), I507 (E) and F508 (F) are shown. Only the shortest distance (< 6 Å) is drawn between two residues. Distance of two atoms is labelled for those polar chemical bonds. For the purpose of illustration, residues 515-516 were omitted from the structures. See other details in Figure S1.

Figure S3. Side-chain interactions of residues 509-513 in the cryo-EM structure of human wild-type CFTR. *A-F*) Side-chain interactions of G509 (A), V510 (B), S511 (C), Y512 (D) and D513 (E) are shown. For further details, see Figures S1 and S2.

Figure S4. Amino acid sequence alignment of CFTR orthologues for residues 501 to 553. Residues that differ from that at the same position in human wild-type CFTR are identified by blue letters and grey background. Percentage similarity was calculated using the equation: (number of matched residues) / (total number of CFTR orthologues [45]) * 100%.

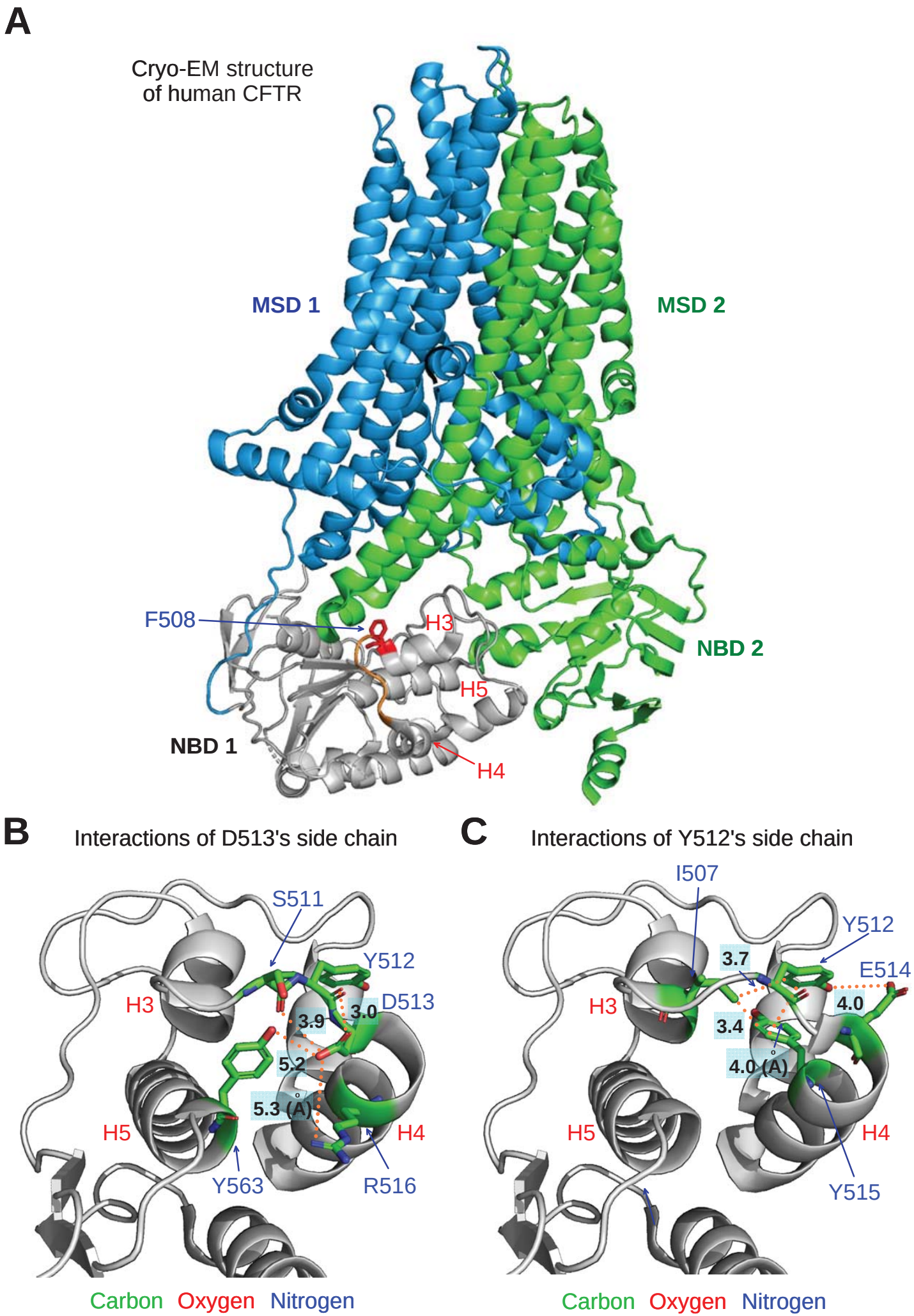
A
Cryo-EM structure
of human CFTR
MSD 1
MSD 2
F508
H3
NBD 2
H5
NBD 1
H4
B
Interactions of D513's side chain
S511
Y512
H3
D513
3.9
3.0
5.2
5.3 (A)
H5
H4
Y563
R516
Carbon Oxygen Nitrogen
C
Interactions of Y512's side chain
I507
Y512
3.7
E514
H3
4.0
3.4
4.0 (A)
H5
H4
Y515
Carbon Oxygen Nitrogen

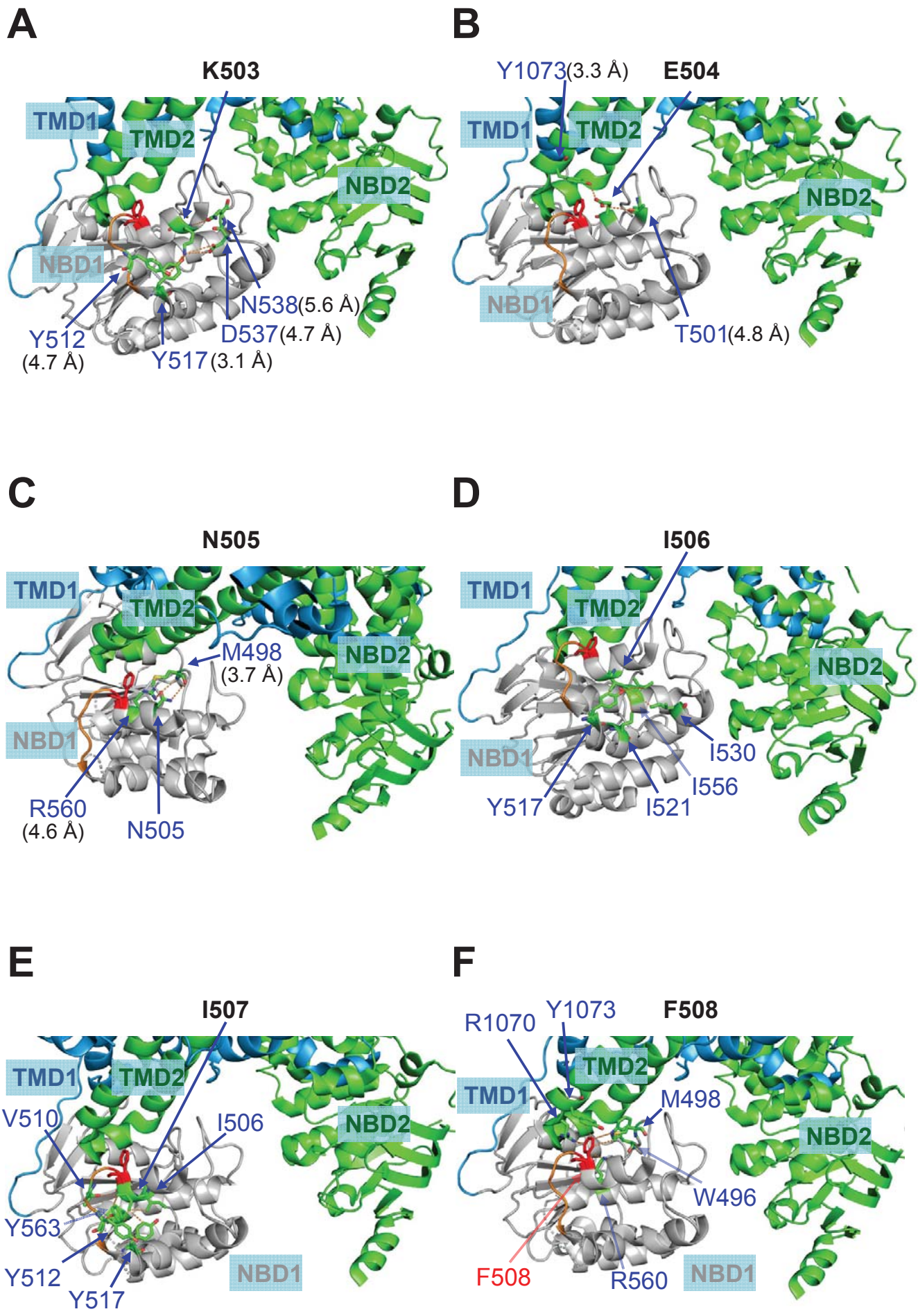
A
K503
TMD1
TMD2
NBD2
NBD1
N538(5.6 Å)
D537(4.7 Å)
Y512
(4.7 Å)
Y517(3.1 Å)
B
Y1073(3.3 Å)
E504
TMD1
TMD2
NBD2
NBD1
T501(4.8 Å)
C
N505
TMD1
TMD2
M498
(3.7 Å)
NBD2
NBD1
R560
(4.6 Å)
N505
D
I506
TMD1
TMD2
NBD2
NBD1
I530
I556
Y517
I521
E
I507
TMD1
TMD2
V510
I506
NBD2
Y563
Y512
Y517
NBD1
F
R1070
Y1073
F508
TMD2
TMD1
M498
NBD2
W496
F508
R560
NBD1

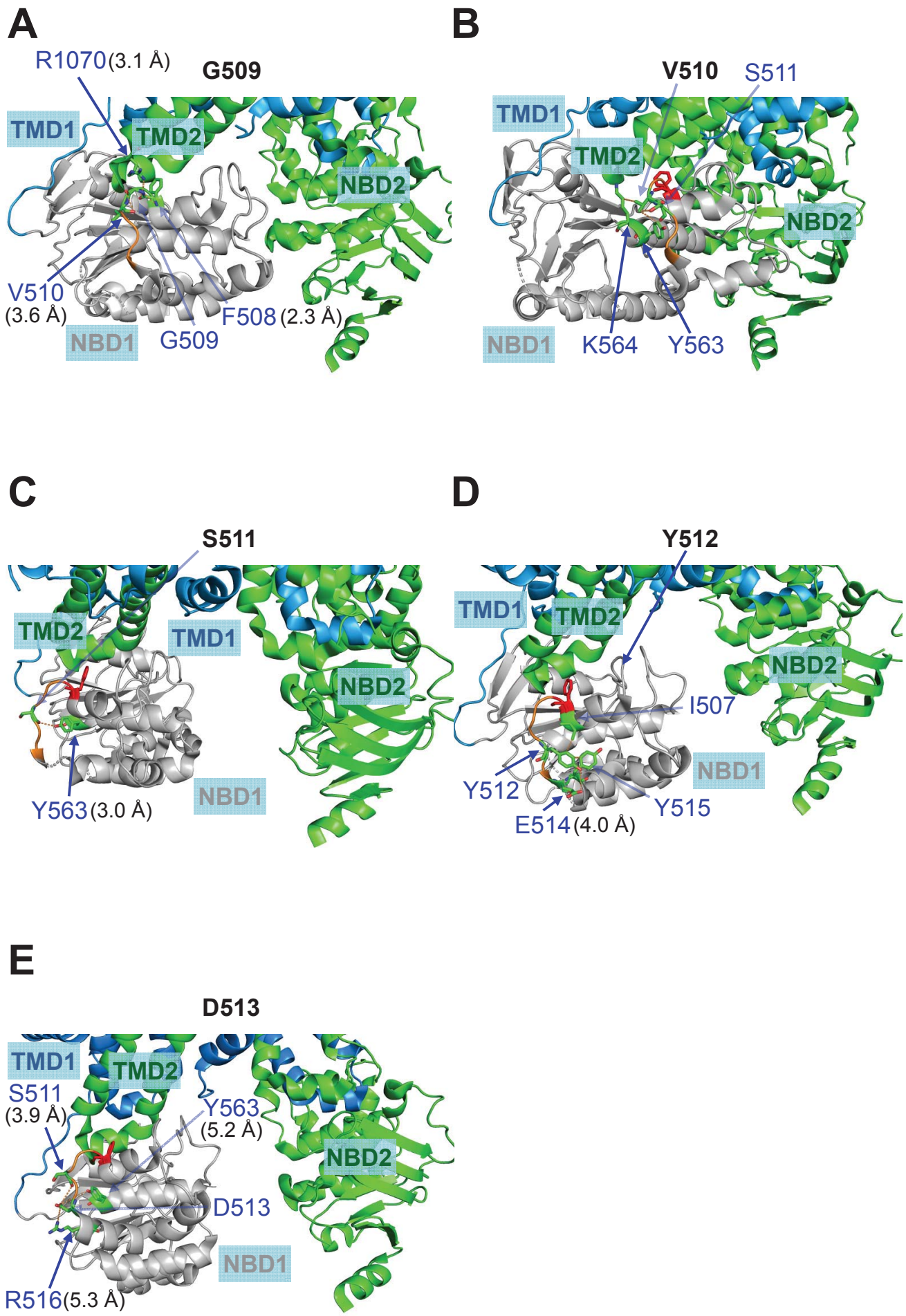
A
R1070 (3.1 Å)
G509
TMD1
TMD2
NBD2
V510
(3.6 Å)
NBD1
G509
F508 (2.3 Å)
B
V510
S511
TMD1
TMD2
NBD2
NBD1
K564
Y563
C
S511
TMD2
TMD1
NBD2
Y563 (3.0 Å)
NBD1
D
Y512
TMD1
TMD2
NBD2
I507
NBD1
Y512
Y515
E514 (4.0 Å)
E
D513
TMD1
TMD2
S511
(3.9 Å)
Y563
(5.2 Å)
NBD2
D513
NBD1
R516 (5.3 Å)

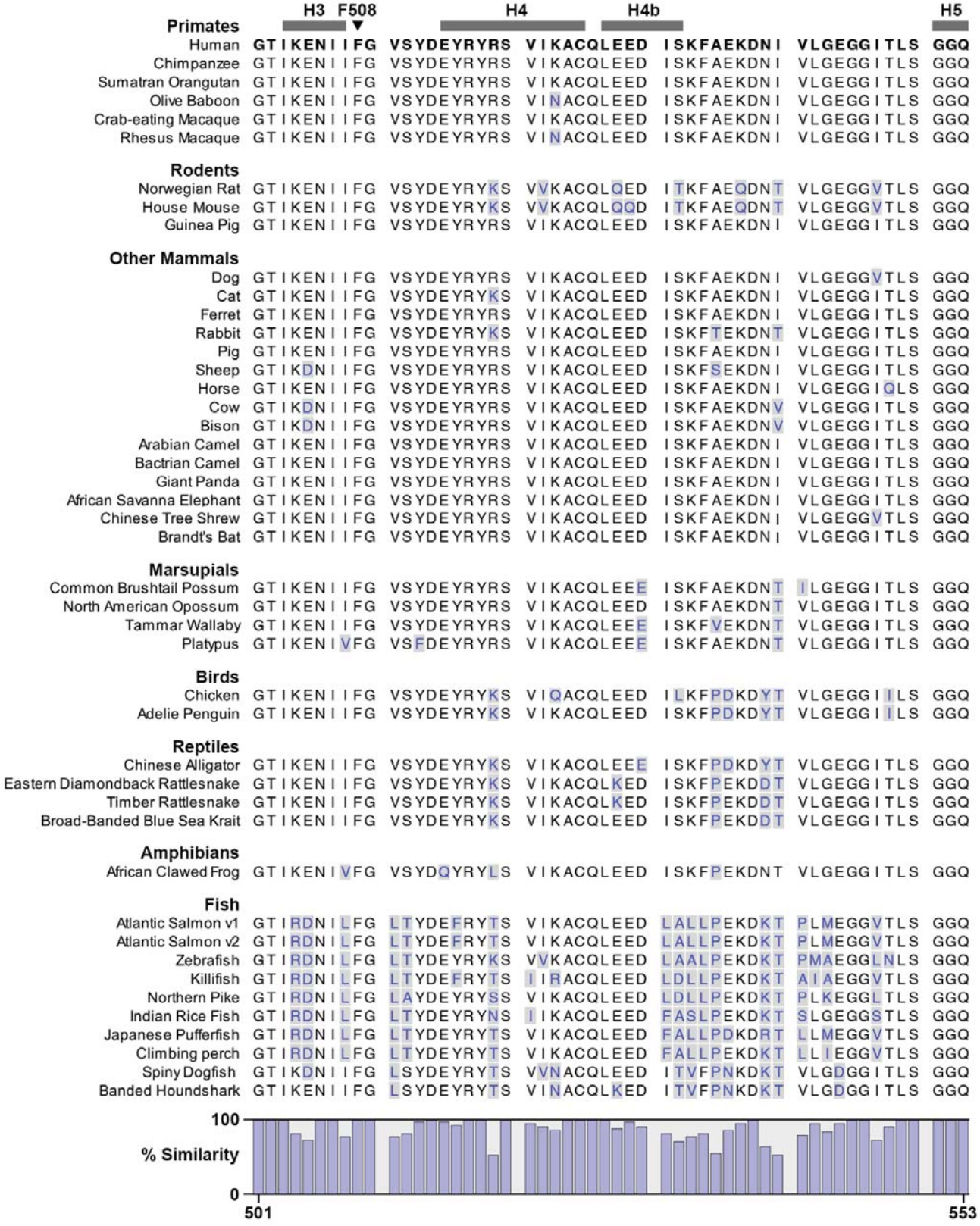
H3
F508
H4
H4b
H5
Primates
Human GTIKENIIFG VSYDEYRYRS VIKACQLEED ISKFAEKDNI VLGEGGITLS GGQ
Chimpanzee GTIKENIIFG VSYDEYRYRS VIKACQLEED ISKFAEKDNI VLGEGGITLS GGQ
Sumatran Orangutan GTIKENIIFG VSYDEYRYRS VIKACQLEED ISKFAEKDNI VLGEGGITLS GGQ
Olive Baboon GTIKENIIFG VSYDEYRYRS VINACQLEED ISKFAEKDNI VLGEGGITLS GGQ
Crab-eating Macaque GTIKENIIFG VSYDEYRYRS VIKACQLEED ISKFAEKDNI VLGEGGITLS GGQ
Rhesus Macaque GTIKENIIFG VSYDEYRYRS VINACQLEED ISKFAEKDNI VLGEGGITLS GGQ
Rodents
Norwegian Rat GTIKENIIFG VSYDEYRYKS VVKACQLQED ITKFAEQDNT VLGEGGVTLS GGQ
House Mouse GTIKENIIFG VSYDEYRYKS VVKACQLQQD ITKFAEQDNT VLGEGGVTLS GGQ
Guinea Pig GTIKENIIFG VSYDEYRYRS VIKACQLEED ISKFAEKDNI VLGEGGITLS GGQ
Other Mammals
Dog GTIKENIIFG VSYDEYRYRS VIKACQLEED ISKFAEKDNI VLGEGGVTLS GGQ
Cat GTIKENIIFG VSYDEYRYKS VIKACQLEED ISKFAEKDNI VLGEGGITLS GGQ
Ferret GTIKENIIFG VSYDEYRYRS VIKACQLEED ISKFAEKDNI VLGEGGITLS GGQ
Rabbit GTIKENIIFG VSYDEYRYKS VIKACQLEED ISKFTEKDNT VLGEGGITLS GGQ
Pig GTIKENIIFG VSYDEYRYRS VIKACQLEED ISKFAEKDNI VLGEGGITLS GGQ
Sheep GTIKDNIIFG VSYDEYRYRS VIKACQLEED ISKFSEKDNI VLGEGGITLS GGQ
Horse GTIKENIIFG VSYDEYRYRS VIKACQLEED ISKFAEKDNI VLGEGGIQLS GGQ
Cow GTIKDNIIFG VSYDEYRYRS VIKACQLEED ISKFAEKDNV VLGEGGITLS GGQ
Bison GTIKDNIIFG VSYDEYRYRS VIKACQLEED ISKFAEKDNV VLGEGGITLS GGQ
Arabian Camel GTIKENIIFG VSYDEYRYRS VIKACQLEED ISKFAEKDNI VLGEGGITLS GGQ
Bactrian Camel GTIKENIIFG VSYDEYRYRS VIKACQLEED ISKFAEKDNI VLGEGGITLS GGQ
Giant Panda GTIKENIIFG VSYDEYRYRS VIKACQLEED ISKFAEKDNI VLGEGGITLS GGQ
African Savanna Elephant GTIKENIIFG VSYDEYRYRS VIKACQLEED ISKFAEKDNI VLGEGGITLS GGQ
Chinese Tree Shrew GTIKENIIFG VSYDEYRYRS VIKACQLEED ISKFAEKDNI VLGEGGVTLS GGQ
Brandt's Bat GTIKENIIFG VSYDEYRYRS VIKACQLEED ISKFAEKDNI VLGEGGITLS GGQ
Marsupials
Common Brushtail Possum GTIKENIIFG VSYDEYRYRS VIKACQLEEE ISKFAEKDNT ILGEGGITLS GGQ
North American Opossum GTIKENIIFG VSYDEYRYRS VIKACQLEED ISKFAEKDNT VLGEGGITLS GGQ
Tammar Wallaby GTIKENIIFG VSYDEYRYRS VIKACQLEEE ISKFVEKDNT VLGEGGITLS GGQ
Platypus GTIKENIVFG VSFDEYRYRS VIKACQLEEE ISKFAEKDNT VLGEGGITLS GGQ
Birds
Chicken GTIKENIIFG VSYDEYRYKS VIQACQLEED ILKFPDKDYT VLGEGGIILS GGQ
Adelie Penguin GTIKENIIFG VSYDEYRYKS VIKACQLEED ISKFPDKDYT VLGEGGIILS GGQ
Reptiles
Chinese Alligator GTIKENIIFG VSYDEYRYKS VIKACQLEEE ISKFPDKDYT VLGEGGITLS GGQ
Eastern Diamondback Rattlesnake GTIKENIIFG VSYDEYRYKS VIKACQLKED ISKFPEKDDT VLGEGGITLS GGQ
Timber Rattlesnake GTIKENIIFG VSYDEYRYKS VIKACQLKED ISKFPEKDDT VLGEGGITLS GGQ
Broad-Banded Blue Sea Krait GTIKENIIFG VSYDEYRYKS VIKACQLEED ISKFPEKDDT VLGEGGITLS GGQ
Amphibians
African Clawed Frog GTIKENIVFG VSYDQYRYLS VIKACQLEED ISKFPEKDNT VLGEGGITLS GGQ
Fish
Atlantic Salmon v1 GTIRDNILFG LTYDEFRYTS VIKACQLEED LALLPEKDKT PLMEGGVTLS GGQ
Atlantic Salmon v2 GTIRDNILFG LTYDEFRYTS VIKACQLEED LALLPEKDKT PLMEGGVTLS GGQ
Zebrafish GTIRDNILFG LTYDEYRYKS VVKACQLEED LAALPEKDKT PMAEGGLNLS GGQ
Killifish GTIRDNILFG LTYDEFRYTS IIRACQLEED LDLLPEKDKT AIAEGGVTLS GGQ
Northern Pike GTIRDNILFG LAYDEYRYSS VIKACQLEED LDLLPEKDKT PLKEGGLTLS GGQ
Indian Rice Fish GTIRDNILFG LTYDEYRYNS IIKACQLEED FASLPEKDKT SLGEGGSTLS GGQ
Japanese Pufferfish GTIRDNILFG LTYDEYRYTS VIKACQLEED FALLPDKDRT LLMEGGVTLS GGQ
Climbing perch GTIRDNILFG LTYDEYRYTS VIKACQLEED FALLPEKDKT LLIEGGVTLS GGQ
Spiny Dogfish GTIKDNIIFG LSYDEYRYTS VVNACQLEED ITVFPNKDKT VLGDGGITLS GGQ
Banded Houndshark GTIKENIIFG LSYDEYRYTS VINACQLKED ITVFPNKDKT VLGDGGITLS GGQ
100
% Similarity
0
501
553